

Intelligent Hybrid Controller for Identification and Control of Micro Permanent-Magnet Synchronous Motor Servo Drive System Using Petri Recurrent-Fuzzy-Neural-Network

FAYEZ F. M. EL-SOUSY

Department of Electrical Engineering

College of Engineering, Salman bin Abdulaziz University

AI-KHARJ, SAUDI ARABIA

Department of Power Electronics and Energy Conversion

Electronics Research Institute

CAIRO, EGYPT

E-mail: f.elsousy@sau.edu.sa, fayez@eri.sci.eg

Abstract: This paper proposes an intelligent hybrid control system (IHCS) for identification and control of micro-permanent-magnet synchronous motor (micro-PMSM) servo drive to achieve high precision tracking performance. The proposed control scheme incorporates a computed torque controller (CTC) based on the sliding-mode technique, a Petri recurrent-fuzzy-neural-network (PRFNN) controller (PRFNNC) and a PRFNN identifier (PRFNNI). First, a CTC is designed to stabilize the micro-PMSM servo drive system. However, particular information about the uncertainties of the micro-PMSM servo drive is required in the CTC law so that the corresponding control performance can not be influenced seriously. Then, to improve the robustness of the servo drive system an IHCS is proposed. In the IHCS, the PRFNNC is used as the main tracking controller to mimic the CTC law and to preserve favorable model-following characteristics while the PRFNNI is utilized to identify the sensitivity information of the micro-PMSM servo drive system required for the PRFNNC. The online adaptive control laws are derived based on the Lyapunov stability theorem, the Taylor linearization technique and the back propagation method so that the stability of the micro-PMSM servo drive system can be guaranteed under occurrence of servo drive uncertainties. A computer simulation is developed to demonstrate the effectiveness of the proposed IHCS. The dynamic performance of the servo drive has been studied under load changes and parameters uncertainties. Accurate tracking response can be obtained due to the powerful on-line learning capability of PRFNN. In addition, the position tracking performance is significantly improved using the proposed IHCS and robustness to external disturbances can be obtained as well. Finally, the simulation results confirm that the IHCS grants robust performance and precise response regardless of load disturbances and micro-PMSM servo drive system parameter uncertainties.

Key-Words: Computed torque control, intelligent control, Lyapunov stability theorem, micro-permanent-magnet synchronous motor, Petri net (PN), recurrent-fuzzy-neural-network, sliding-mode control.

1 Introduction

Recently, the processing techniques of micro-electromechanical systems (MEMS) have been applied in micro-motors to reduce size and power dissipation. These micro-motors cannot provide a large torque or power as the traditional motors. Nevertheless, micro-motors have several advantages. For example, they are smaller in size, have low power dissipation and light weight. As a result, micro-motors are well suited to some specific applications. The micro-motors types are micro-DC motors, micro-switched reluctance motors, micro-induction motors and micro-permanent magnet synchronous motors (micro-PMSMs). Due to the requirements of extremely small actuators in medical community and semiconductor industries, micro-motors are downscaled to millimeter scale with the

help of micromachining and MEMS techniques [1]. High-speed micro-PMSMs are an important category of micro-motors with a diameter of less than 10 mm. In the past few years the manufacturers of high-precision motors have developed a series of products of micro-PMSMs. As commercial products, micro PMSMs are available in size as small as 2 mm in diameter by 5 mm in length. The micro-PMSM has better performance than the other micro-motors owing to its high power density, high output efficiency, high maneuverability and reliability, high speed operation capability and good robustness [2], [3]. In addition, micro-PMSMs are considered very important actuators for many industrial applications. The typical applications are micro autonomous robots; micro recording and data storage devices; reconnaissance and security equipment;

pumping/dispensing systems; medical diagnostic, treatment, and surgical devices; cell biology research tools; and chemical analysis apparatus. They can also be important power driving devices in MEMS [4]. A micro-PMSM drive system generally consists of a micro-PMSM, a micro-gear head, control action and power electronics. A position sensor is necessary for the applications with high-performance position control. In such a system mechanical parts and devices are already available in micro-scale. However a challenge to the system designers is how to downscale controllers to the comparable sizes of micro-motors with the comparable control performance. For many applications, a small-sized electronic controller for micro-motors is very important [1]-[4].

In recent years, control of micro-motors is gaining the attention of researchers since various new micro-motors in different operating principles have been developed based on micromachining and MEMS techniques [2]. Researches have reported the control of MEMS electrostatic induction micro-motors and micro-PMSMs [5]-[24]. These two types of micro-motors are the two directions in the development of micro-motors: electrostatic principle and magnetic principle. Small and effective control systems with micro-motors will greatly promote the practical applications of various micro-motors. The micro-PMSM has different characteristics from the traditional PMSM. For example, its inductance is smaller than 1mH and its resistance is larger than 50 Ω . As a result, the micro-PMSM is usually operated in discontinuous current conditions. Moreover, control of the micro-PMSM is more difficult than that of the traditional PMSM owing to its size limitation and small inductance.

Some papers have focused on the research of micro-motors [5]-[8]. In [5], the design for a magnetic induction micro-motor that offers high power densities is introduced. A detailed description of the fabrication and testing of both the stator and the tethered rotor of a magnetic induction micro machine is presented [6]. A fully nonlinear magnetic model of the micro machine based on a finite-difference time-domain method has been developed. This modeling approach is quite convenient for the study of many electromagnetic phenomena and is especially suited for high-frequency operation regimes and nonlinear material applications [7]. In [9], the concept, simulation, fabrication and testing of linear variable reluctance micro-motor with compensated attraction force have been studied.

On the other hand, several papers have discussed the control methods of micro-motors. In [10] a six-phase multilevel inverter for a micro-motor is

proposed. A novel adjustable micro-permanent magnet synchronous motor control system without using a rotor position/speed sensor is introduced [11], [12]. The sensorless techniques and applications of the micro-motor have been studied [14]. In addition, an H_∞ controller and a rotor position estimator for a micro-permanent magnet synchronous motor control system are developed [13], [15].

Several researchers have investigated micro-motor control systems [1], [16]-[24]. A three-dimensional characteristic analysis of a micro-motor is proposed [17], the design and fabrication of a precision micro-motor for surgery [16]. However, most of the papers published focus on the design, characteristics, drive and applications of micro-motors [1], [2], [16]-[18]. Only a few papers focus on the controller design of the micro-motors. Some researchers have done the theoretical analysis and computer simulations [19]-[21] on micro-motor control. In addition, an advanced control algorithms for micro-motors is presented in [19]. A proposed closed-loop micro-motor control system in which only the simulated results were included in [20]. An intelligent hybrid control system using robust PFNN controller and identifier for micro-PMSM servo drive system is designed and analyzed [21]. An adaptive inverse controller for a micro-permanent magnet synchronous control system is proposed in [22]. The adaptive inverse controller is constructed by an adaptive model and an adaptive controller. In [23], a sensorless technique for micro-permanent magnet synchronous motor control system with a wide adjustable speed range is presented, in which an optimal control algorithm is proposed to design the speed controller. An optimal position controller combined with a tuning parameter feed-forward controller, is proposed to implement a motion control system using micro-permanent magnet synchronous motors [24]. In [47], a robust position sensorless control method based on sliding-mode observer for high-speed micro-PMSM, which is suitable for wide speed range applications, is implemented.

Intelligent control techniques in much research have been developed to improve the performance of dynamic systems and to deal with the nonlinearities and uncertainties using fuzzy logic, neural network and/or the hybrid of them [21], [25]-[27], [43]. The concept of incorporating fuzzy logic into a neural network (NN) has grown into a popular research topic. In contrast to the pure neural network or fuzzy system, the fuzzy-neural-network (FNN) possesses both their advantages; it combines the capability of fuzzy reasoning in handling uncertain information and the capability of NNs in learning from the process [28]-[32]. On the other hand, the recurrent

fuzzy-neural-network (RFNN), which naturally involves dynamic elements in the form of feedback connections used as internal memories, has been studied in the past few years [31, 32]. In recent years, Petri net has found widely applications in modeling and controlling discrete event dynamic systems [33]-[36]. For the last decades, Petri net (PN) has developed into a powerful tool for modeling, analysis, control, optimization, and implementation of various engineering systems [37]-[42]. In [21], an intelligent hybrid control system using robust Petri recurrent-fuzzy-neural-network (PRFNN) controller and PRFNN identifier for micro-PMSM servo drive system is designed and analyzed to achieve high precision tracking performance. The proposed control scheme combines a computed torque controller (CTC) based on the sliding-mode technique, a PRFNN controller and a PRFNN identifier. In [42], the designed of a network structure by introducing PN into RFNN to form a dynamic Petri RFNN (DPRFNN) scheme for the path-tracking control of a nonholonomic mobile robot is presented.

In this paper, an intelligent hybrid control system (IHCS) is proposed for identification and control the rotor position of the micro-PMSM servo drive. The configuration of the proposed IHCS for micro-PMSM servo drive is shown in Fig.1. First, based on the principle of CTC with sliding-mode technique, a position tracking controller is designed and the stability analysis is studied. Although the tracking and regulation position control performance can be realized using the CTC, the performance of the micro-PMSM servo drive system is influenced seriously due to the uncertainties including the inevitable approximation errors, unknown disturbances of the micro-PMSM servo drive system. To solve this problem and in order to control the rotor position of the micro-PMSM effectively, an IHCS is proposed. The IHCS consists of a PRFNN controller (PRFNCC), PRFNN identifier (PRFNNI) and a CTC based on the sliding-mode technique. The PRFNCC is used as the main tracking controller to mimic the CTC law and the PRFNNI is used to provide the sensitivity information of the drive system to the PRFNCC. The online adaptive control laws are derived based on the Lyapunov stability theorem, Taylor linearization technique and back propagation method so that the stability of the micro-PMSM servo drive can be guaranteed. A computer simulation is developed to demonstrate the effectiveness of the proposed IHCS. The dynamic performance of the servo drive has been studied under load changes and parameters uncertainties. The numerical simulation results are

given to demonstrate the effectiveness of the proposed IHCS.

This paper is organized as follows. Section 2 presents the field-orientation control and dynamic analysis of the micro-PMSM servo drive as well as the problem formulation. Section 3 provides the description, design and stability analysis of the CTC based on the sliding-mode technique. The description of the PRFNN model and the online learning algorithm signal analysis is introduced in Section 4. In addition, the IHCS and its online learning algorithms for the PRFNN controller and PRFNN identifier are given in Section 5. The design and stability analysis of the proposed control scheme is introduced in Section 6. The validity of the design procedure and the robustness of the proposed control scheme are verified by means of computer simulation results as given in Section 7. Conclusions are introduced in Section 8.

2 Modeling of the micro-PMSM

The voltage equations of the stator windings in the rotating reference frame can be expressed in (1) and (2). Then, using FOC and setting d-axis current as zero, the electromagnetic torque is obtained as given in (3) and (4) [21]. The parameters of the micro-PMSM are listed in Table (1).

$$V_{qs}^r = R_s i_{qs}^r + L_{ss} \frac{d}{dt} i_{qs}^r + \omega_r L_{ss} i_{ds}^r + \omega_r \lambda_m' \quad (1)$$

$$V_{ds}^r = R_s i_{ds}^r + L_{ss} \frac{d}{dt} i_{ds}^r - \omega_r L_{ss} i_{qs}^r \quad (2)$$

The electromagnetic torque can be expressed as:

$$T_e = (3/2) \cdot (P/2) \cdot \lambda_m i_{qs}^r = K_t i_{qs}^r \quad (3)$$

$$T_e = J_m \left(\frac{2}{P} \right) \frac{d^2}{dt^2} \theta_r + \beta_m \left(\frac{2}{P} \right) \frac{d}{dt} \theta_r + T_L \quad (4)$$

From (3) and (4), the mechanical dynamics can be simplified as:

$$\ddot{\theta}_r = -\frac{\beta_m}{J_m} \left(\frac{2}{P} \right) \dot{\theta}_r + \frac{K_t}{J_m} \left(\frac{2}{P} \right) i_{qs}^{r*} - \frac{2}{P} \cdot \frac{1}{J_m} \cdot T_L \quad (5)$$

$$\ddot{\theta}_r = A_m \dot{\theta}_r + B_m \cdot U(t) + D_m \cdot T_L \quad (6)$$

where $U(t) = i_{qs}^{r*}(t)$ is the control effort, $A_m = -(\beta_m / J_m) \cdot (P/2)$, $B_m = K_t / (J_m \cdot P/2)$ and $D_m = -(P/2) \cdot (1 / J_m)$.

Now, assume that the parameters of the micro-PMSM are well known and the external load disturbance is absent, rewriting (6) can represent the model of the servo drive system.

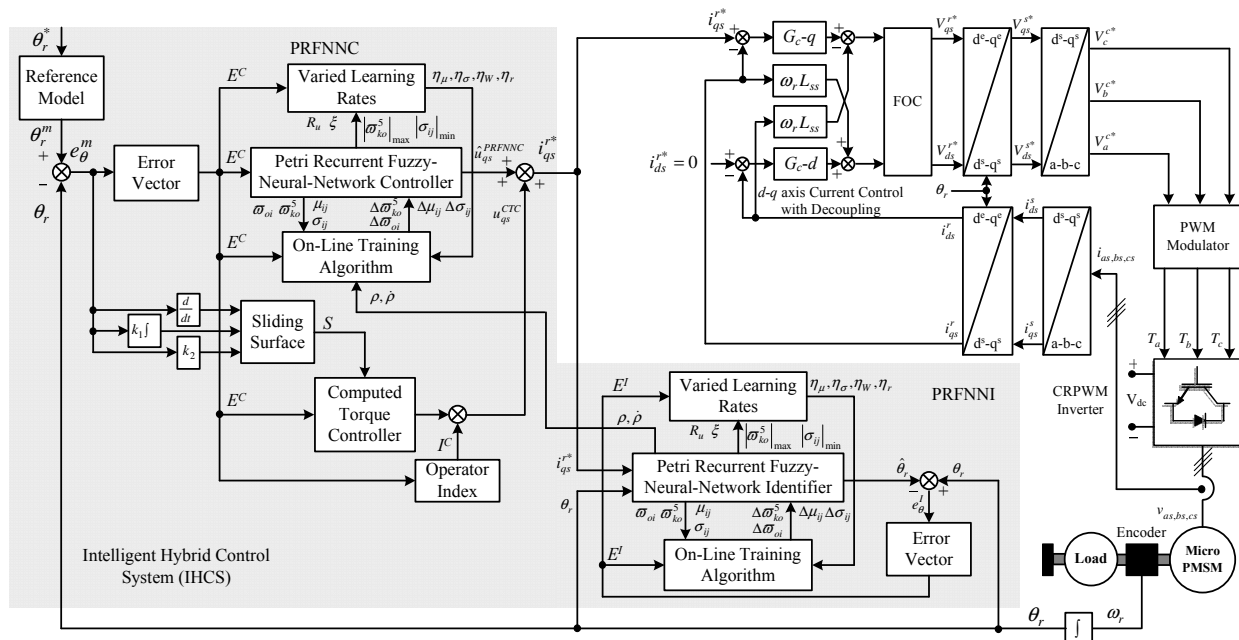


Fig. 1 Structure of the proposed intelligent hybrid control system using PRFNN for micro-PMSM servo drive

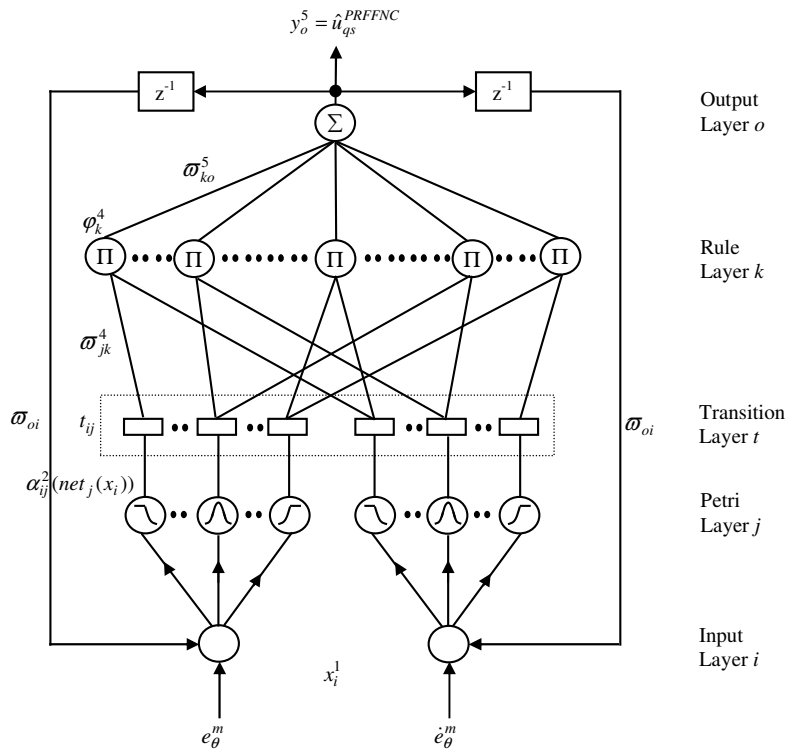


Fig. 2 Structure of five-layer PRFNN

$$\ddot{\theta}_r(t) = A_m \cdot \dot{\theta}_r(t) + B_m \cdot U(t) \quad (7)$$

By considering the dynamics in (6) with parameter variations, disturbance load and unpredictable uncertainties will give:

$$\ddot{\theta}_r(t) = (A_n + \Delta A_m) \dot{\theta}_r(t) + (B_n + \Delta B_m) \cdot U(t) + (D_n + \Delta D_m) \cdot T_L \quad (8)$$

$$\ddot{\theta}_r(t) = A_n \dot{\theta}_r(t) + B_n \cdot U(t) + \Gamma(t) \quad (9)$$

where A_n , B_n and D_n are the nominal parameters of A_m , B_m and D_m respectively. ΔA_m , ΔB_m , ΔD_m and T_L are the uncertainties due to mechanical parameters J_m and β_m , and $\Gamma(t)$ is the lumped parameter uncertainty and is defined as:

$$\Gamma(t) = \Delta A_m \dot{\theta}_r(t) + \Delta B_m \cdot U(t) + (D_{mn} + \Delta D_m) T_L \quad (10)$$

The bound of the lumped parameter uncertainty is assumed to be given, that is,

$$|\Gamma(t)| \leq \delta^{SMC} \quad (11)$$

where δ^{SMC} is a given positive constants.

Table 1 Parameters of the micro-PMSM

Parameter	Symbol	Value
Nominal power	P_n	1.2 W (3-phase)
Stator inductance	L_{ss}	0.59 mH
Stator resistance	R_s	75.4 Ω
Voltage constant	λ_m	3474 rpm/V
Number of poles	P	2
Rotor inertia	J_m	4.9x10 ⁻⁹ kg.m ²
Friction coefficient	β_m	2x10 ⁻⁶ N.m/rad/sec
Nominal speed	N_r	35940 rpm
Rated torque	T_e	0.00044 N.m
Rated current	I	0.105 A
Rated voltage	V_{L-L}	12 V
Torque constant	K_t	0.00275 N.m/A

3 Computed Torque Control Based on the Sliding-Mode Technique

The CTC is utilized to linearize the nonlinear equation of micro-PMSM servo drive motion by cancellation of some, or all, nonlinear terms. The control problem is to find a control law so that the rotor position $\theta_r(t)$ can track the desired position $\theta_r^m(t)$. To achieve this control objective, we define a tracking error vector as follows:

$$E = [\theta_r^m - \theta_r \quad \dot{\theta}_r^m - \dot{\theta}_r]^T = [e_\theta^m \quad \dot{e}_\theta^m]^T \quad (12)$$

where $\theta_r^m(t)$ and $\dot{\theta}_r^m(t)$ are the desired rotor position and speed of the micro-PMSM servo drive system; $e_\theta^m(t)$ and $\dot{e}_\theta^m(t)$ denote the rotor position and speed error. Now, a sliding surface is defined as

$$S(t) = \dot{e}_\theta(t) + k_2 e_\theta(t) + k_1 \int e_\theta(\tau) d\tau \quad (13)$$

where the positive constants k_1 and k_2 are designed based on the desired drive system dynamics such as rise time, overshoot and settling time. Differentiating $S(t)$ with respect to time will give:

$$\dot{S}(t) = \ddot{e}_\theta^m(t) + k_2 \dot{e}_\theta^m(t) + k_1 e_\theta^m(t) \quad (14)$$

Using the differentiation of the error position function, $e_\theta(t) = \theta_r^m(t) - \theta_r(t)$, and (9) and substituting into (14) will yield:

$$\dot{S}(t) = [\ddot{\theta}_r^m(t) - A_m \dot{\theta}_r(t) - B_m U(t) - \Gamma(t) + k_2 \dot{e}_\theta(t) + k_1 e_\theta(t)] \quad (15)$$

The tracking problem is to find a control law $U(t)$ so that the rotor position remaining on the sliding surface for all $t > 0$. In the design of the SMC system, the ideal equivalent control law, which determines the dynamics of the servo drive system on the switching surface, is derived. The ideal equivalent control law is derived from $\dot{S}(t) = 0$. Applying this equality to (15) will provide

$$\dot{S}(t) \Big|_{U=U_{eq}} = 0 \quad (16)$$

Substituting (15) into (16) will yield

$$[\ddot{\theta}_r^m(t) - A_m \dot{\theta}_r(t) - B_m U(t) - \Gamma(t) + k_2 \dot{e}_\theta(t) + k_1 e_\theta(t)] = 0 \quad (17)$$

Solving (17), we can obtain

$$\begin{aligned} U_{eq}(t) &= U_{qs}^{CTC}(t) \\ &= B_m^{-1} [\ddot{\theta}_r^m(t) - A_m \dot{\theta}_r(t) - \Gamma(t) + k_2 \dot{e}_\theta(t) + k_1 e_\theta(t)] \\ &= B_m^{-1} [\ddot{\theta}_r^m(t) - A_m \dot{\theta}_r(t) - \Gamma(t) + KE] \end{aligned} \quad (18)$$

where $K = [k_1 \quad k_2]$, in which k_1 and k_2 are positive constants.

Thus, for $\dot{S}(t) = 0$, the dynamic of the system on the sliding surface a $t \geq 0$ is given by

$$\ddot{e}_\theta^m(t) + k_2 \dot{e}_\theta^m(t) + k_1 e_\theta^m(t) = 0 \quad (19)$$

Suppose the control gain K is chosen such that all roots of the characteristic polynomial of (19) lie strictly in the open left half of the complex plane. This implies that the position tracking error will converge to zero when time tends to infinity, i.e. the micro-PMSM servo drive states can track the desired trajectory asymptotically. However, the parameter variations of the micro-PMSM are difficult to measure and the exact value of the external load disturbance is also difficult to know in advance for practical applications. Though, if the micro-PMSM parameters are perturbed, the CTC law can not guarantee the performance specified by (19). Moreover, the stability of the micro servo drive may be destroyed. To ensure the system performance, designed by (19), despite of the existence the uncertain dynamics, a new CTC law is proposed. If the bound of the lumped parameter uncertainty is assumed to be $|\Gamma(t)| \leq \delta^{SMC}$.

Theorem 1: The globally asymptotic stability of (15) is guaranteed if the CTC law based on the sliding-mode technique is designed as (20)

$$\begin{aligned} U_{qs}^*(t) &= B_m^{-1} [\ddot{\theta}_r^m(t) - A_m \dot{\theta}_r(t) + k_2 \dot{e}_\theta(t) \\ &\quad + k_1 e_\theta(t) - \delta^{SMC} \text{sgn}(S)] \end{aligned} \quad (20)$$

where $\text{sgn}(\cdot)$ is a sign function.

Proof: Define the Lyapunov function candidate as:

$$V_1(S(t)) = \frac{1}{2} S^2(t) \quad (21)$$

Taking the derivative of the Lyapunov function and using (21), we can get

$$\begin{aligned} \dot{V}_1(S(t)) &= S(t)\dot{S}(t) \\ &= S(t)[\dot{\theta}_r^m(t) - A_{mm}\dot{\theta}_r(t) - B_m U(t) \\ &\quad - \Gamma(t) + k_2 \dot{e}_\theta(t) + k_1 e_\theta(t)] \\ &= S(t)\Gamma(t) - |S(t)|\delta^{SMC} \\ &\leq |S(t)|\Gamma(t) - |S(t)|\delta^{SMC} \\ &\leq -|S(t)|[\delta^{SMC} - |\Gamma(t)|] < 0 \end{aligned} \quad (22)$$

Therefore, the sliding condition can be assured throughout the whole control period. According to the Lyapunov theorem [44], [45], the globally asymptotic stability of the sliding-mode control system can be guaranteed. To trade off the robustness and the chattering phenomena, a conservative gain δ^{SMC} is always selected by trial and error. The incorrect selection of this control gain will yield to the deviation from the sliding surface and cause chattering phenomena. Therefore, for chattering elimination and to ensure the stability of the micro-PMSM servo drive despite the existence of the uncertain dynamics and external load disturbance, an IHCS is proposed in the following section.

4 Petri Recurrent Fuzzy Neural Network (PRFNN)

Recently, the RFNN has been proven to be a powerful technique in the discipline of system control. However, real-time implementation may be difficult or impossible due to heavy computation burden if huge network parameters to be tuned or inference strategies are complicated. In order to overcome this problem, the concept of a PN is incorporated into a RFNN to reduce redundant or inefficient computation for improving the control reliability. The description of the Petri RFNN (PRFNN) structure, online learning algorithm, and convergence analyses are given in the following sections.

4.1 PRFNN Structure

The architecture of the proposed five-layer PRFNN configuration is shown in Fig. 2, which comprises the input layer (the i layer), Petri layer (the j layer), transition layer (the t layer), rule layer (the k layer) and output layer (the o layer) is adopted to implement the PRFNN in this paper. Moreover, z^{-1} represents a time-delay and the output of the PRFNN is recurrent to the input layer through a time delay. The major difference between the RFNN [27], [31], [32] and the proposed PRFNN is the transition layer.

The signal propagation and the basic function in each layer are introduced as follows [21], [42].

1) Layer 1: Input Layer

The nodes in layer 1 transmit the input signals to the next layer. For every node i in the input layer, the net input and the net output can be represented as:

$$net_i^1 = \prod_o x_i^1(N) \varpi_{oi} y_o^5(N-1) \quad (23)$$

$$y_i^1(N) = f_i^1(net_i^1(N)) = net_i^1(N) \quad i=1,2 \quad (24)$$

$$x_1^1 = e_\theta^m(t), \quad x_1^1 = i_{qs}^{r*}(t)$$

$$x_2^1 = \dot{e}_\theta^m(t), \quad x_2^1 = \theta_r(t) \quad (25)$$

where x_i^1 represents the i th input to the node of layer 1, N denotes the number of iterations, ϖ_{oi} is the recurrent weights for the units of the output layer and y_o^5 is the output of the PRFNN.

2) Layer 2: Petri Layer

In this layer, the output of each node is used to represent tokens with the same Gaussian function. For the j th node (Petri node), the input and output of the Petri node can be described as follows:

$$net_j^2(x_i) = -\frac{(x_i^2 - \mu_{ij})^2}{\sigma_{ij}^2} \quad (26)$$

$$\alpha_{ij}^2(net_j^2(x_i)) = \exp(net_j^2(x_i)) \quad (27)$$

where μ_{ij} and σ_{ij} ($i = 1, \dots, n; j = 1, \dots, N_p$), respectively, are the mean and standard deviation of the Gaussian function in the j th term of the i th input variable x_i to the node of this layer, N_p is the number of Petri nodes with respect to the input nodes and n is the total number of input nodes.

3) Layer 3: Transition Layer

The transition layer of the PRFNN is used to produce tokens and also makes use of competition learning laws to select suitable fired nodes as follows:

$$t_{ij}^3 = \begin{cases} 1, & \alpha_{ij}^2(net_j^2(x_i)) \geq d_{th} \\ 0, & \alpha_{ij}^2(net_j^2(x_i)) < d_{th} \end{cases} \quad (28)$$

where t_{ij} is the transition and d_{th} is a dynamic threshold value varied with the corresponding error.

4) Layer 4: Rule Layer

Each node k in layer 4 (rule layer) is denoted by \prod , which multiplies the incoming signals and outputs the result of the product. For the k th nodes:

$$net_k^4(\alpha_{ij}^2) = \begin{cases} \prod_{i=1}^n \varpi_{jk}^4 \alpha_{ij}^2(net_j^2(x_i)), & t_{ij}^2 = 1 \\ 0, & t_{ij}^2 = 0 \end{cases} \quad (29)$$

$$\begin{aligned} \phi_k^4(\alpha_{ij}^2) &= f_k^4(net_k^4(\alpha_{ij}^2)) = net_k^4(\alpha_{ij}^2) \\ k &= 1, \dots, N_r \end{aligned} \quad (30)$$

where α_{ij}^2 represents the j th input to the node of the rule layer (layer 4), $\bar{\omega}_k^4$ is the weights between the transition layer and the rule layer. These weights are also assumed to be unity; and N_r is the total number of rules.

5) Layer 5: Output Layer

The single node o in the output layer is denoted by Σ , which computes the overall output as the summation of all incoming signals as follows:

$$net_o^5 = \sum_{k=1}^{N_r} \bar{\omega}_{ko}^5 \phi_k^4 (\alpha_{ij}^2) \quad (31)$$

$$y_o^5 = f_o^5 (net_o^5) = net_o^5 \quad o = 1 \quad (32)$$

$$y_o^5 = u_{qs}^{*PRFNNC} (t) = W^T \Psi \quad (33)$$

where the connecting weight $\bar{\omega}_{ko}^5$ is the output action strength of the o th output associated with the k th rule, ϕ_k^4 represents the k th input to the node of output layer. $W(\bar{\omega}_{oi}, \bar{\omega}_{ko})$, $\bar{\omega}_{ko}^5 = [\bar{\omega}_{1o}^5 \ \bar{\omega}_{2o}^5 \ \dots \ \bar{\omega}_{ko}^5]^T$ and $\bar{\omega}_{io} = [\bar{\omega}_{1o} \ \bar{\omega}_{2o} \ \dots \ \bar{\omega}_{ko}]^T$ are the collections of the adjustable parameters $(\bar{\omega}_{oi}, \bar{\omega}_{ko})$, in which $\bar{\omega}_{ko}^5$ and $\bar{\omega}_{oi}$ are initialized to be zero and adjusted during on-line operation and $\Psi = \phi_k^4 = [\phi_1^4 \ \phi_2^4 \ \dots \ \phi_k^4]^T$, in which ϕ_k^4 is determined by the Petri and transition layers.

4.2 On-line Training Algorithm for PRFNN

The central part of the on-line training algorithm for the PRFNN concerns how to recursively obtain a gradient vector in which each element in the learning algorithm is defined as the derivative of an energy function with respect to a parameter of the network using the chain rule. Since the gradient vector is calculated in the direction opposite the flow of the output of each node [21], [42], [43], the method is generally referred to as the backpropagation learning rule. To describe the on-line learning algorithm of the PRFNN using the supervised gradient-descent method, the energy function is chosen as:

$$E_\theta = \frac{1}{2} [(\theta^m - \theta) + (\dot{\theta}^m - \dot{\theta})]^2 \quad (34)$$

$$= \frac{1}{2} [(e^m)^2 + (\dot{e}^m)^2]$$

where $\theta^m(t)$ is the desired response, $\theta(t)$ is the actual output and e^m is the error signal between the desired response and the actual output.

The learning algorithm based on the back-propagation is described as follows.

1) Layer 5:

In the output layer (layer 5), the error term to be propagated is calculated as:

$$\delta_o^5 = -\frac{\partial E_\theta}{\partial y_o^5} = -\left(\left[\frac{\partial E_\theta}{\partial e^m} \cdot \frac{\partial e^m}{\partial y_o^5} \right] + \left[\frac{\partial E_\theta}{\partial \dot{e}^m} \cdot \frac{\partial \dot{e}^m}{\partial y_o^5} \right] \right)$$

$$= -\left(\left[\frac{\partial E_\theta}{\partial e^m} \cdot \frac{\partial e^m}{\partial \theta} \cdot \frac{\partial \theta}{\partial y_o^5} \right] + \left[\frac{\partial E_\theta}{\partial \dot{e}^m} \cdot \frac{\partial \dot{e}^m}{\partial \dot{\theta}} \cdot \frac{\partial \dot{\theta}}{\partial y_o^5} \right] \right)$$

$$= \left(e^m \frac{\partial \theta}{\partial y_o^5} + \dot{e}^m \frac{\partial \dot{\theta}}{\partial y_o^5} \right) \quad (35)$$

The weight is updated by the amount:

$$\Delta \bar{\omega}_{ko}^5 = -\eta_W \frac{\partial E_\theta}{\partial \bar{\omega}_{ko}^5}$$

$$= \left[-\eta_W \frac{\partial E_\theta}{\partial y_o^5} \right] \left(\frac{\partial y_o^5}{\partial net_o^5} \cdot \frac{\partial net_o^5}{\partial \bar{\omega}_{ko}^5} \right) = \eta_W \delta_o^5 \phi_k^4 \quad (36)$$

where η_W is the learning rate parameter of the connecting weights of the output layer of the PRFNN.

The weights of the output layer (layer 5) are updated according to the following equation.

$$\bar{\omega}_{ko}^5 (N + 1) = \bar{\omega}_{ko}^5 (N) + \Delta \bar{\omega}_{ko}^5 \quad (37)$$

where N denotes the number of iterations.

2) Layer 4:

In rule layer (layer 4), only the error term needs to be computed and propagated because the weights in this layer are unity.

$$\delta_k^4 = -\frac{\partial E_\theta}{\partial net_k^4} = -\frac{\partial E_\theta}{\partial \phi_k^4}$$

$$= \begin{cases} -\frac{\partial E_\theta}{\partial y_o^5} \frac{\partial y_o^5}{\partial \phi_k^4} & \phi_k^4 \neq 0 \\ 0 & \phi_k^4 = 0 \end{cases} \quad (38)$$

3) Layer 2:

In the Petri layer (layer 2), the error term is calculated as follows:

$$\delta_j^2(x_i) = -\frac{\partial E_\theta}{\partial net_j^2(x_i)}$$

$$= \left(-\frac{\partial E_\theta}{\partial y_o^5} \cdot \frac{\partial y_o^5}{\partial \phi_k^4} \right) \left(\frac{\partial \phi_k^4}{\partial \alpha_{ij}^2 (net_j^2(x_i))} \right) \quad (39)$$

$$\frac{\partial \alpha_{ij}^2 (net_j^2(x_i))}{\partial net_j^2(x_i)} = \begin{cases} \sum_k \delta_k^4 \phi_k^4 & t_{ij}^2 = 1 \\ 0 & t_{ij}^2 = 0 \end{cases}$$

The update laws of μ_{ij} and σ_{ij} are given by:

$$\Delta \mu_{ij} = -\eta_\mu \frac{\partial E_\theta}{\partial \mu_{ij}} = \eta_\mu \left[-\frac{\partial E_\theta}{\partial y_o^5} \frac{\partial y_o^5}{\partial net_j^2(x_i)} \frac{\partial net_j^2(x_i)}{\partial \mu_{ij}} \right]$$

$$= \eta_\mu \delta_j^2(x_i) \frac{2(x_i - \mu_{ij})}{(\sigma_{ij})^2} \quad (40)$$

$$\begin{aligned}\Delta\sigma_{ij} &= -\eta_{\sigma} \frac{\partial E_{\theta}}{\partial \sigma_{ij}} = \eta_{\sigma} \left[-\frac{\partial E_{\theta}}{\partial y_o^5} \frac{\partial y_o^5}{\partial net_j^2(x_i)} \frac{\partial net_j^2(x_i)}{\partial \sigma_{ij}} \right] \\ &= \eta_{\sigma} \delta_j^2(x_i) \frac{2(x_i - \mu_{ij})^2}{(\sigma_{ij})^2}\end{aligned}\quad (41)$$

where η_{μ} and η_{σ} are the learning rate parameters of the mean and standard deviation of the Gaussian function. The mean and standard deviation of the Petri layer are updated as follows:

$$\mu_{ij}(N+1) = \mu_{ij}(N) + \Delta\mu_{ij}(N) \quad (42)$$

$$\sigma_{ij}(N+1) = \sigma_{ij}(N) + \Delta\sigma_{ij}(N) \quad (43)$$

The update law of the recurrent weight ϖ_{oi} can be obtained by the following equation:

$$\begin{aligned}\Delta\varpi_{oi} &= -\eta_r \frac{\partial E_{\theta}}{\partial \varpi_{oi}} = \left[-\eta_r \frac{\partial E_{\theta}}{\partial y_o^5} \frac{\partial y_o^5}{\partial net_j^2(x_i)} \frac{\partial net_j^2(x_i)}{\partial \varpi_{oi}} \right] \\ &= -\eta_r \delta_j^2(x_i) \frac{2(x_i - \mu_{ij})}{(\sigma_{ij})^2} \mu_{ij}(N-1)\end{aligned}\quad (44)$$

where η_r is the learning rate parameters of the recurrent weights. The recurrent weights are updated as follows:

$$\varpi_{oi}(N+1) = \varpi_{oi}(N) + \Delta\varpi_{oi}(N) \quad (45)$$

5 Intelligent Hybrid Control System Using PRFNN

In this section, the description and stability analysis of the IHCS for the micro-PMSM servo drive are introduced. Although the desired tracking and regulation position control performance can be realized using the CTC at the nominal micro-PMSM parameters, the performance of the servo drive system still sensitive to parameter variations. To solve this problem and in order to control the rotor position of the micro-PMSM effectively, an IHCS is proposed. The configuration of the proposed IHCS, which combines a PRFNNC, a PRFNNI and a CTC with sliding-mode, for micro-PMSM servo drive is shown in Fig.1. The hybrid control law is assumed to take the following form:

$$u_{qs}^*(t) = i_{qs}^{r*}(t) = u_{qs}^{PRFNNC}(t) + u_{qs}^{CTC}(t) \quad (46)$$

where $u_{qs}^{PRFNNC}(t)$ is the PRFNNC and $u_{qs}^{CTC}(t)$ is the computed torque controller based on the sliding-mode technique.

5.1 Petri Recurrent Fuzzy Neural Network Controller (PRFNNC)

The PRFNNC is used as the main tracking controller to mimic the CTC law. The inputs of the PRFNNC

are e_{θ}^m and \dot{e}_{θ}^m . The PRFNNC is trained by the backpropagation algorithm. The learning process is to minimize the tracking error e_{θ}^m .

5.2 Petri Recurrent Fuzzy Neural Network Identifier (PRFNNI)

The PRFNNI is used to mimic the dynamic characteristics of the micro-PMSM servo drive. The inputs to the PRFNNI are the reference current command i_{qs}^{r*} and the output of the servo drive θ_r . The PRFNNI is trained by the backpropagation algorithm to estimate the rotor position of the servo drive, $\hat{\theta}_r$, with the actual rotor position of the servo drive, θ_r , used as the desired response. The learning process is to minimize the tracking error e_{θ}^l and provide the Jacobian of the micro-PMSM servo drive system for the training of the PRFNNC.

5.3 On-line Training Algorithm of the PRFNNC and PRFNNI

To describe the on-line learning algorithm of the PRFNNC using the supervised gradient-descent method, the energy function is chosen as [21]:

$$E_{\theta}^C = \frac{1}{2}[(\theta_r^m - \theta_r) + (\dot{\theta}_r^m - \dot{\theta}_r)]^2 = \frac{1}{2}[(e_{\theta}^m)^2 + (\dot{e}_{\theta}^m)^2] \quad (47)$$

where $\theta_r^m(t)$ is the desired position, $\theta_r(t)$ is the actual rotor position and e_{θ}^m is the error signal between the desired and the actual rotor position.

During the learning process of the PRFNNC, the error term to be propagated in (35) is calculated as:

$$\begin{aligned}\delta_o^5 &= -\frac{\partial E_{\theta}^C}{\partial y_o^5} = -\left(\left[\frac{\partial E_{\theta}^C}{\partial e_{\theta}^m} \cdot \frac{\partial e_{\theta}^m}{\partial y_o^5} \right] + \left[\frac{\partial E_{\theta}^C}{\partial \dot{e}_{\theta}^m} \cdot \frac{\partial \dot{e}_{\theta}^m}{\partial y_o^5} \right] \right) \\ &= -\left(\left[\frac{\partial E_{\theta}^C}{\partial e_{\theta}^m} \cdot \frac{\partial e_{\theta}^m}{\partial \theta_r} \cdot \frac{\partial \theta_r}{\partial y_o^5} \right] + \left[\frac{\partial E_{\theta}^C}{\partial \dot{e}_{\theta}^m} \cdot \frac{\partial \dot{e}_{\theta}^m}{\partial \dot{\theta}_r} \cdot \frac{\partial \dot{\theta}_r}{\partial y_o^5} \right] \right) \quad (48) \\ &= \left(e_{\theta}^m \frac{\partial \theta_r}{\partial y_o^5} + \dot{e}_{\theta}^m \frac{\partial \dot{\theta}_r}{\partial y_o^5} \right) = e_{\theta}^m \rho + \dot{e}_{\theta}^m \dot{\rho}\end{aligned}$$

The reminder of the on-line learning algorithm of the PRFNNC is the same as given by (35-45).

To describe the on-line learning algorithm of the PRFNNI using the supervised gradient-descent method, the energy function is chosen as:

$$E_{\theta}^l = \frac{1}{2}[(\theta_r - \hat{\theta}_r) + (\dot{\theta}_r - \dot{\hat{\theta}}_r)]^2 = \frac{1}{2}[(e_{\theta}^l)^2 + (\dot{e}_{\theta}^l)^2] \quad (49)$$

where $\hat{\theta}_r(t)$ is the estimated rotor position, $\theta_r(t)$ is the actual rotor position and e_{θ}^l is the error signal between the estimated rotor position and the actual position.

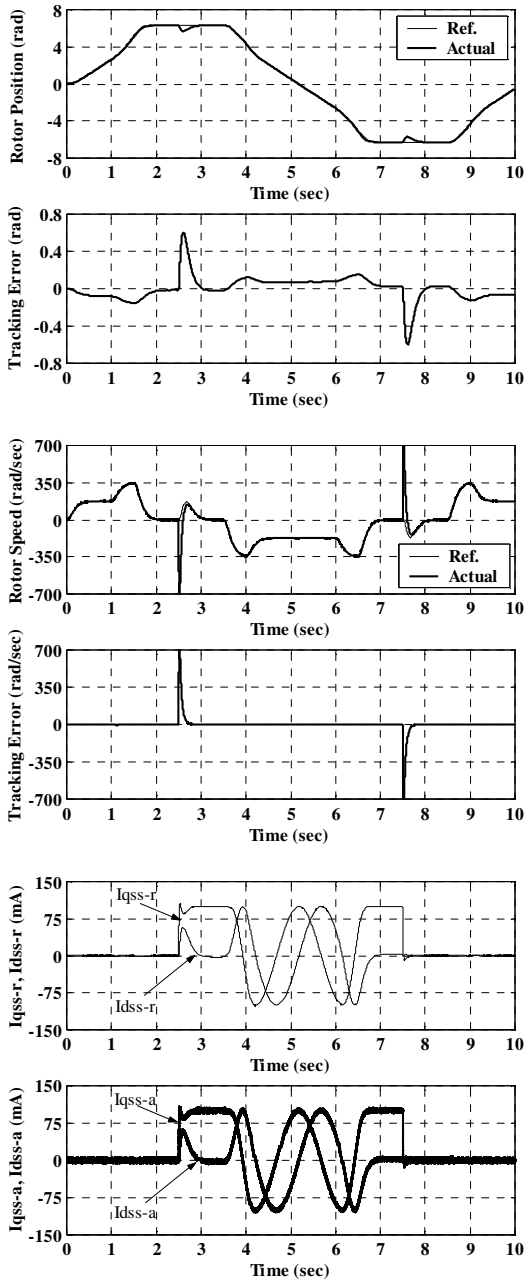


Fig. 3 Dynamic response of the micro-PMSM drive system for a reference model of 2π rad and subsequent loading of 0.5 mNm using CTC

During the learning process of the PRFNNI, the error term to be propagated in (35) is calculated as:

$$\begin{aligned} \delta_o^5 &= -\frac{\partial E_\theta^l}{\partial y_o^5} = -\left(\left[\frac{\partial E_\theta^l}{\partial e_\theta^l} \cdot \frac{\partial e_\theta^l}{\partial y_o^5} \right] + \left[\frac{\partial E_\theta^l}{\partial \hat{e}_\theta^l} \cdot \frac{\partial \hat{e}_\theta^l}{\partial y_o^5} \right] \right) \\ &= -\left(\left[\frac{\partial E_\theta^l}{\partial e_\theta^l} \cdot \frac{\partial e_\theta^l}{\partial \hat{\theta}_r} \cdot \frac{\partial \hat{\theta}_r}{\partial y_o^5} \right] + \left[\frac{\partial E_\theta^l}{\partial \hat{e}_\theta^l} \cdot \frac{\partial \hat{e}_\theta^l}{\partial \hat{\theta}_r} \cdot \frac{\partial \hat{\theta}_r}{\partial y_o^5} \right] \right) \quad (50) \\ &= \left(e_\theta^l \frac{\partial \hat{\theta}_r}{\partial y_o^5} + \hat{e}_\theta^l \frac{\partial \hat{\theta}_r}{\partial y_o^5} \right) = e_\theta^l + \hat{e}_\theta^l \end{aligned}$$

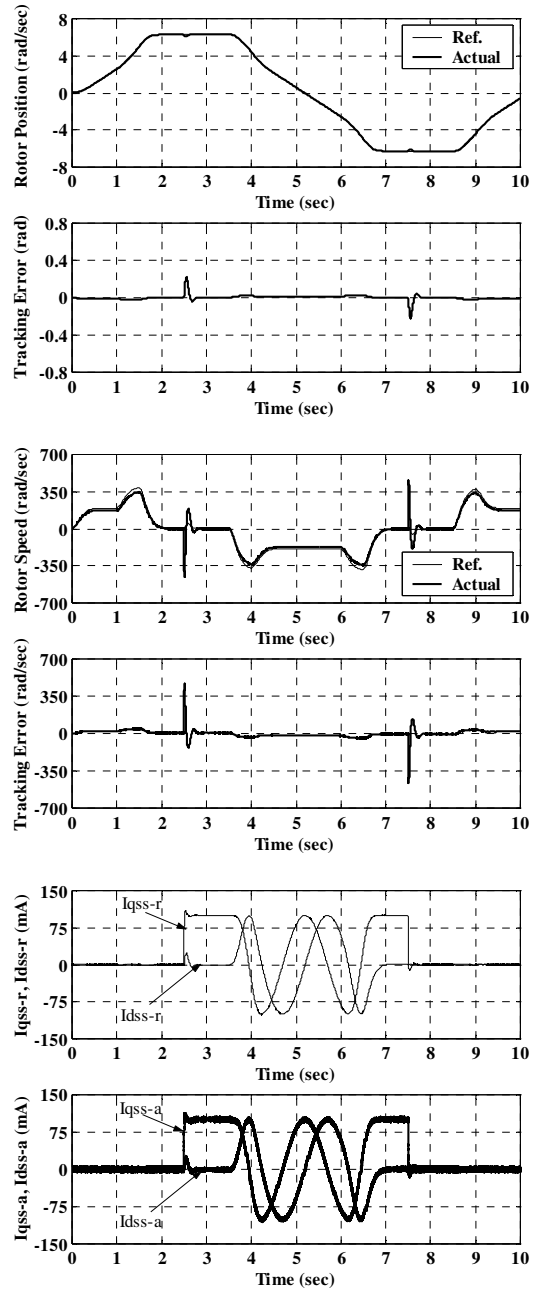


Fig. 4 Dynamic response of the micro-PMSM drive system for a reference model of 2π rad and subsequent loading of 0.5 mNm using PRFNNC

The reminder of the on-line learning algorithm of the PRFNNI is the same as given by (35-45). The exact calculation of the micro-PMSM Jacobian $\partial \theta_r / \partial i_{qs}^{r*}$ and $\partial \hat{\theta}_r / \partial i_{qs}^{r*}$ can be determined using the PRFNNI when the identification error becomes small enough, i.e. $\hat{\theta}_r \cong \theta_r$ and $\hat{e}_\theta \cong e_\theta$. From (50) and (35-45), the Jacobian of the micro-PMSM servo drive system is calculated as follows:

$$\frac{\partial \theta_r}{\partial i_{qs}^{r*}} \cong \frac{\partial \hat{\theta}_r}{\partial i_{qs}^{r*}} = \frac{\partial y_o^5}{\partial x_1^1} = \frac{\partial y_o^5}{\partial net_o^5} \cdot \frac{\partial net_o^5}{\partial \varphi_k^4(\alpha_{ij}^2)}$$

$$\frac{\partial \phi_k^4(\alpha_{ij}^2)}{\partial \alpha_{ij}^2(\text{net}_j^2(x_i))} \cdot \frac{\partial \alpha_{ij}^2(\text{net}_j^2(x_i))}{\partial \text{net}_j^2(x_i)} \cdot \frac{\partial \text{net}_j^2(x_i)}{\partial x_i^1} \cong \rho \quad (51)$$

$$\frac{\partial \hat{\theta}_r}{\partial i_{qs}^{r*}} \cong \frac{\partial \hat{\theta}_r}{\partial i_{qs}^{r*}} = \frac{\partial y_o^5}{\partial x_2^1} = \frac{\partial y_o^5}{\partial \text{net}_o^5} \cdot \frac{\partial \text{net}_o^5}{\partial \phi_k^4(\alpha_{ij}^2)}$$

$$\frac{\partial \phi_k^4(\alpha_{ij}^2)}{\partial \alpha_{ij}^2(\text{net}_j^2(x_i))} \cdot \frac{\partial \alpha_{ij}^2(\text{net}_j^2(x_i))}{\partial \text{net}_j^2(x_i)} \cdot \frac{\partial \text{net}_j^2(x_i)}{\partial x_2^1} \cong \dot{\rho} \quad (52)$$

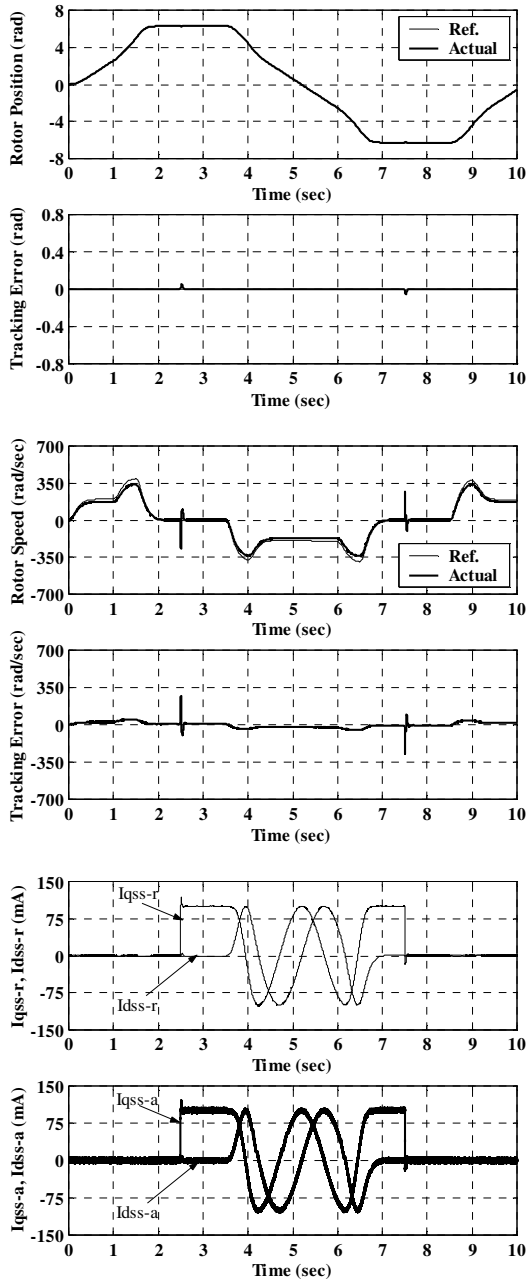


Fig. 5 Dynamic response of the micro-PMSM drive system for a reference model of 2π rad and subsequent loading of 0.5 mNm using IHCS

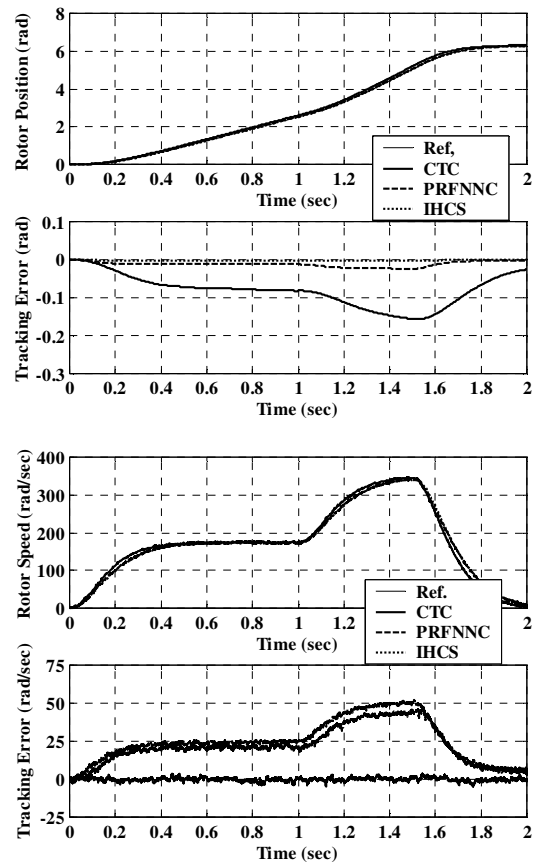


Fig. 6 Comparison the model-following tracking response using CTC, PRFNNC and IHCS for the micro-PMSM servo drive system

5.4 Convergence Analyses of the PRFNN

Selection of the values for the learning rates η_w , η_μ , η_σ and η_r has a significant effect on the network performance. In order to train the PRFNN effectively, adaptive learning rates, which guarantee the convergence of tracking errors and identification based on the analyses of a discrete-type Lyapunov function are derived as [32].

6 Design and Stability Analysis of the Intelligent Hybrid Control System

In order to efficiently control the rotor position of the micro-PMSM drive system, an IHCS, which comprises a PRFNNC and a PRFNNI and their associated network parameters tuning algorithm, is proposed to increase the robustness of the micro-PMSM drive system. The intelligent hybrid control system for the micro-PMSM drive is shown in Fig. 1, in which the reference model is used as the closed loop transfer function of the drive system with PID position controller [21]. The PRFNN is designed to mimic the CTC controller in (20) and to increase the robustness of the micro-PMSM drive system. Moreover, the PRFNN parameters tuning laws are

derived in the sense of Lyapunov stability theorem [44], [45] to ensure the PRFNN conversion, as well as the stability of the micro-PMSM servo drive system. Assume that according to universal approximation property, there exist an optimal PRFNNC controller $u_{qs}^{*PRFNNC}$ to learn the CTC law u_{qs}^{CTC} such that

$$u_{qs}^{CTC} = u_{qs}^{*PRFNNC}(E, W^*, \mu^*, \sigma^*) + \varepsilon = W^{*T} \Psi^* + \varepsilon \quad (53)$$

where ε is a minimum reconstructed error; and W^* , μ^* and σ^* are the optimal parameters of W , μ and σ , respectively, in the PRFNN. The PRFNN control law is assumed take the following form:

$$U_{qs}^* = \hat{u}_{qs}^{PRFNNC}(E, \hat{W}, \hat{\mu}, \hat{\sigma}) = \hat{W}^T \hat{\Psi} \quad (54)$$

where \hat{W} , $\hat{\mu}$ and $\hat{\sigma}$ are the estimated values of the optimal parameters as provided by the tuning algorithms that will be introduced later. Subtracting (54) from (53), the approximation error, \tilde{u} , is defined as:

$$\tilde{u} = u_{qs}^{CTC} - \hat{u}_{qs}^{PRFNNC} = W^{*T} \Psi^* + \varepsilon - \hat{W}^T \hat{\Psi} = \tilde{W}^T \Psi^* + \hat{W}^T \tilde{\Psi} + \varepsilon \quad (55)$$

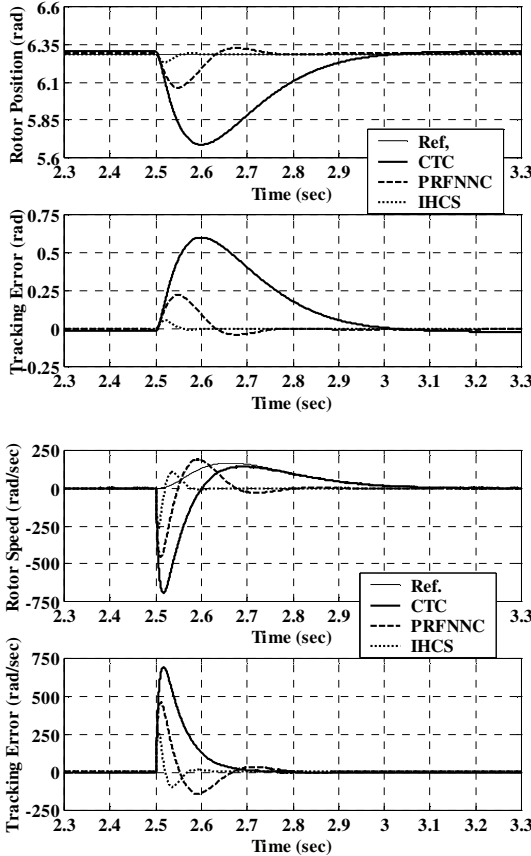


Fig. 7 Comparison the load regulation characteristics using CTC, PRFNNC and IHCS for the micro-PMSM servo drive system under subsequent loading of 0.5 mNm

where $\tilde{W} = (W^* - \hat{W})$ and $\tilde{\Psi} = (\Psi^* - \hat{\Psi})$. The weights of the PRFNN are updated online to make its output approximate the CTC law u_{qs}^{CTC} accurately. To achieve this goal, the linearization technique is used to transform the nonlinear output of PRFNN into partially linear form so that the Lyapunov theorem extension can be applied. The expansion of $\tilde{\Psi}$ in Taylor series is obtained as follows:

$$\tilde{\Psi} = \begin{bmatrix} \tilde{\Psi}_1 \\ \tilde{\Psi}_2 \\ \vdots \\ \tilde{\Psi}_j \end{bmatrix} = \begin{bmatrix} \frac{\partial \Psi_1}{\partial \mu} \\ \frac{\partial \Psi_2}{\partial \mu} \\ \vdots \\ \frac{\partial \Psi_j}{\partial \mu} \end{bmatrix}^T \Big|_{\mu=\hat{\mu}} \tilde{\mu} + \begin{bmatrix} \frac{\partial \Psi_1}{\partial \sigma} \\ \frac{\partial \Psi_2}{\partial \sigma} \\ \vdots \\ \frac{\partial \Psi_j}{\partial \sigma} \end{bmatrix}^T \Big|_{\sigma=\hat{\sigma}} \tilde{\sigma} + \Xi \equiv \Psi_{\mu}^T \tilde{\mu} + \Psi_{\sigma}^T \tilde{\sigma} + \Xi \quad (56)$$

where

$$\Psi_{\mu} = \left[\frac{\partial \Psi_1}{\partial \mu} \quad \frac{\partial \Psi_2}{\partial \mu} \quad \dots \quad \frac{\partial \Psi_j}{\partial \mu} \right]^T \Big|_{\mu=\hat{\mu}}, \quad \Psi_{\sigma} = \left[\frac{\partial \Psi_1}{\partial \sigma} \quad \frac{\partial \Psi_2}{\partial \sigma} \quad \dots \quad \frac{\partial \Psi_j}{\partial \sigma} \right]^T \Big|_{\sigma=\hat{\sigma}}$$

$\tilde{\mu} = (\mu^* - \hat{\mu})$, $\tilde{\sigma} = (\sigma^* - \hat{\sigma})$ and Ξ is a vector of higher order terms and assumed to be bounded by a positive constant. Rewriting (56), one can obtain

$$\Psi^* = \hat{\Psi} + \Psi_{\mu}^T \tilde{\mu} + \Psi_{\sigma}^T \tilde{\sigma} + \Xi \quad (57)$$

From (55) and (57), we can obtain

$$\begin{aligned} \tilde{u} &= W^{*T} \Psi^* + \varepsilon - \hat{W}^T \hat{\Psi} \\ &= W^{*T} [\hat{\Psi} + \Psi_{\mu}^T \tilde{\mu} + \Psi_{\sigma}^T \tilde{\sigma} + \Xi] - \hat{W}^T \hat{\Psi} + \varepsilon \\ &= (W^* - \hat{W})^T \hat{\Psi} + (\tilde{W} + \hat{W}) \Psi_{\mu}^T \tilde{\mu} + (\tilde{W} + \hat{W}) \Psi_{\sigma}^T \tilde{\sigma} \\ &\quad + W^{*T} \Xi + \varepsilon \\ &= \tilde{W}^T \hat{\Psi} + \tilde{W} \Psi_{\mu}^T \tilde{\mu} + \hat{W} \Psi_{\mu}^T \tilde{\mu} + \tilde{W} \Psi_{\sigma}^T \tilde{\sigma} + \hat{W} \Psi_{\sigma}^T \tilde{\sigma} \\ &\quad + W^{*T} \Xi + \varepsilon \\ &= \tilde{W}^T \hat{\Psi} + \hat{W} \Psi_{\mu}^T \tilde{\mu} + \hat{W} \Psi_{\sigma}^T \tilde{\sigma} + \gamma \end{aligned} \quad (58)$$

where $\gamma = \tilde{W} \Psi_{\mu}^T \tilde{\mu} + \tilde{W} \Psi_{\sigma}^T \tilde{\sigma} + W^{*T} \Xi + \varepsilon$ is the uncertain term and is assumed to be bounded. According to (9), (20), (57) and (58), the error dynamics can be represented as

$$\begin{aligned} \dot{E} &= B_n^{-1} (\tilde{u} - KE + \delta^{SMC} \text{sgn}(S) - \Gamma) \\ &= B_n^{-1} (\tilde{W}^T \hat{\Psi} + \hat{W} \Psi_{\mu}^T \tilde{\mu} + \hat{W} \Psi_{\sigma}^T \tilde{\sigma} + \gamma - KE \\ &\quad + \delta^{SMC} \text{sgn}(S) - \Gamma) \\ &= B_n^{-1} (\tilde{W}^T \hat{\Psi} + \hat{W} \Psi_{\mu}^T \tilde{\mu} + \hat{W} \Psi_{\sigma}^T \tilde{\sigma} - KE \\ &\quad + \delta^{SMC} \text{sgn}(S) - \bar{\gamma}) \end{aligned} \quad (59)$$

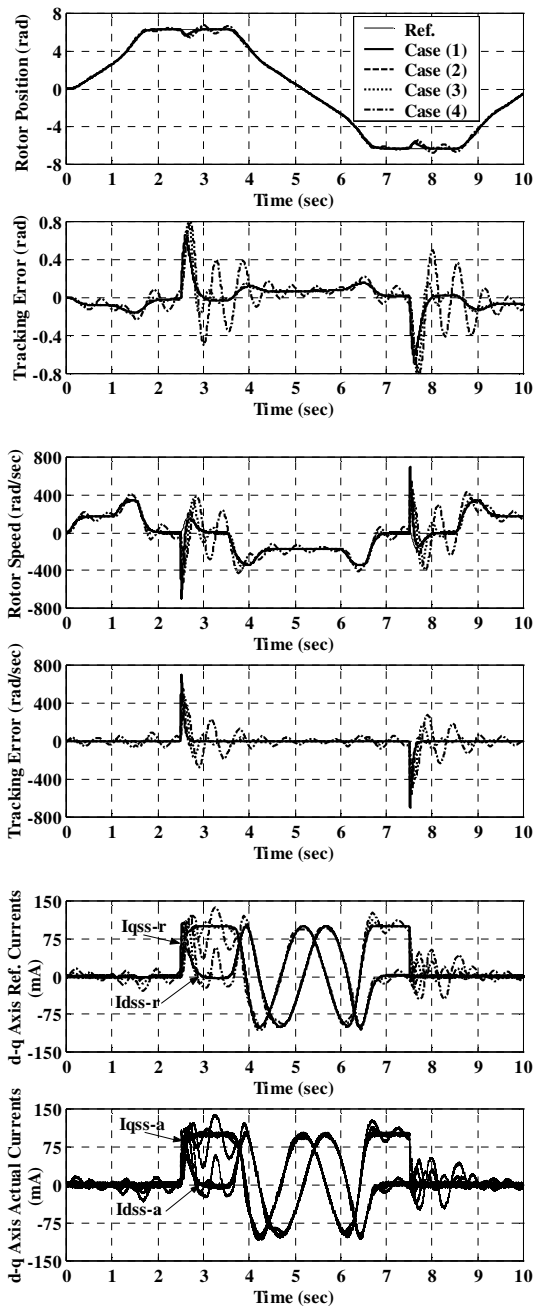


Fig. 8 Dynamic response of the micro-PMSM drive system for a reference model of 2π rad and subsequent loading of 0.5 mNm using CTC at different cases (1~4) of parameter uncertainties

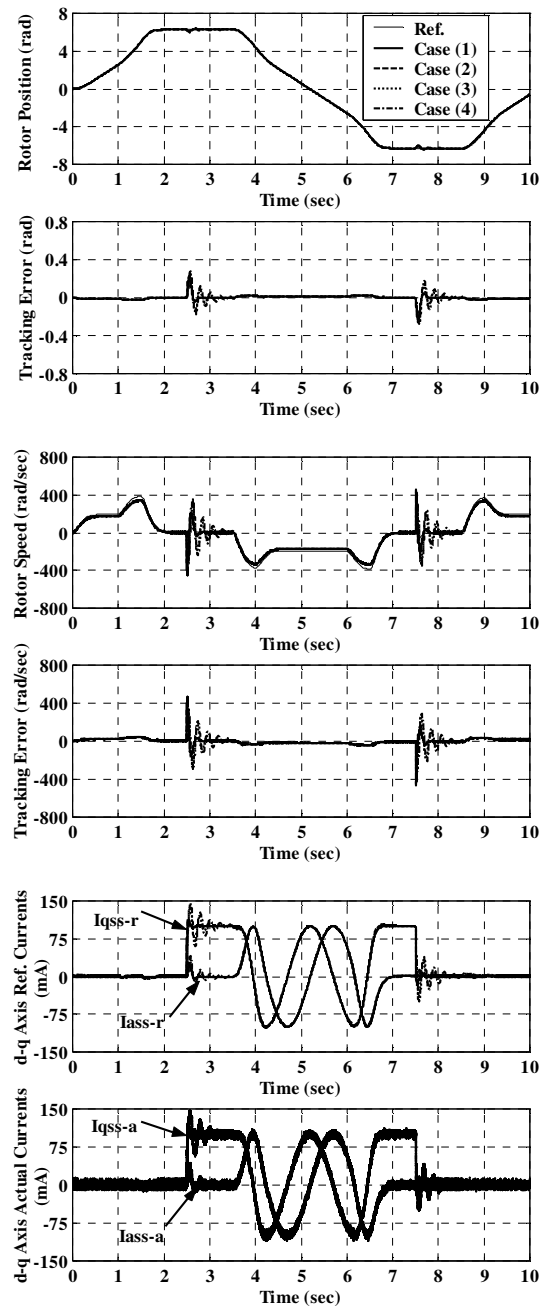


Fig. 9 Dynamic response of the micro-PMSM drive system for a reference model of 2π rad and subsequent loading of 0.5 mNm using PRFNNC at different cases (1~4) of parameter uncertainties

where the uncertain term $\bar{\gamma} = (\Gamma - \gamma)$ is assumed to be bounded (i.e. $|\bar{\gamma}| < \rho$).

Theorem 2: Consider the micro-PMSM servo drive system represented by (9), if the intelligent controller is designed as (54), in which the adaptation laws of the PRFNN are designed as (60)-(62), as a result, the stability of the IHCS can be guaranteed.

$$\dot{\hat{W}} = \eta_w E^T \hat{\Psi}^T \quad (60)$$

$$\dot{\hat{\mu}} = \eta_\mu E^T \hat{W}^T \hat{\Psi}_\mu^T \quad (61)$$

$$\dot{\hat{\sigma}} = \eta_\sigma E^T \hat{W}^T \hat{\Psi}_\sigma^T \quad (62)$$

where η_w , η_μ and η_σ are positive learning rates.

Proof: To minimize the error function and to derive the adaptation laws of W , μ and σ for the intelligent hybrid control system, a Lyapunov function is defined as:

$$V_2(E, \tilde{W}, \tilde{\mu}, \tilde{\sigma}, t) = \frac{1}{2} E^T B_m E + \frac{1}{2\eta_W} \tilde{W}^T \tilde{W} + \frac{1}{2\eta_\mu} \tilde{\mu}^T \tilde{\mu} + \frac{1}{2\eta_\sigma} \tilde{\sigma}^T \tilde{\sigma} \quad (63)$$

By taking the derivative of the Lyapunov function (63) and using (59), it is obtained that

$$\begin{aligned} \dot{V}_2(E, \tilde{W}, \tilde{\mu}, \tilde{\sigma}, t) &= E^T B_m \dot{E} + \frac{1}{\eta_\Theta} \tilde{W}^T \dot{\tilde{W}} + \frac{1}{\eta_\mu} \tilde{\mu}^T \dot{\tilde{\mu}} + \frac{1}{\eta_\sigma} \tilde{\sigma}^T \dot{\tilde{\sigma}} \\ &= E^T B_n \{ B_n^{-1} [\tilde{W}^T \hat{\Psi} + \hat{W} \Psi_\mu^T \tilde{\mu} + \hat{W} \Psi_\sigma^T \tilde{\sigma} - KE + \delta^{SMC} \text{sgn}(S) + \bar{\gamma}] \} - \frac{1}{\eta_W} \tilde{W}^T \dot{\tilde{W}} \\ &\quad - \frac{1}{\eta_\mu} \tilde{\mu}^T \dot{\tilde{\mu}} - \frac{1}{\eta_\sigma} \tilde{\sigma}^T \dot{\tilde{\sigma}} \\ &= -KE^T E + \delta^{SMC} E^T \text{sgn}(S) - E^T \bar{\gamma} \\ &\quad - \left[\tilde{W}^T \left(\frac{1}{\eta_W} \dot{\tilde{W}} - \hat{\Psi} E^T \right) \right] - \left(\frac{1}{\eta_\mu} \dot{\tilde{\mu}} - \hat{W} \Psi_\mu^T E^T \right) \tilde{\mu}^T \\ &\quad - \left(\frac{1}{\eta_\sigma} \dot{\tilde{\sigma}} - \hat{W} \Psi_\sigma^T E^T \right) \tilde{\sigma}^T \end{aligned} \quad (64)$$

If the adaptation laws for the PRFNN parameters are designed as (60)-(62) and the selection of δ^{SMC} equals to $|\bar{\gamma}|$, then (64) can be rewritten as:

$$\begin{aligned} \dot{V}_2(E, \tilde{W}, \tilde{\mu}, \tilde{\sigma}, t) &= -KE^T E + \delta^{SMC} E^T \text{sgn}(S) - E^T \bar{\gamma} \\ &\leq -KE^T E + \delta^{SMC} E^T \text{sgn}(S) - E^T \text{sgn}(S) \|\bar{\gamma}\| \quad (65) \\ &= -KE^T E + E^T \text{sgn}(S) [\delta^{SMC} - \|\bar{\gamma}\|] \\ &\leq -KE^T E \end{aligned}$$

Since $\dot{V}_2(E, \tilde{W}, \tilde{\mu}, \tilde{\sigma}, t) \leq 0$, $V_2(E, \tilde{W}, \tilde{\mu}, \tilde{\sigma}, t)$ is a negative semi-definite function (i.e. $V_2(E, \tilde{W}, \tilde{\mu}, \tilde{\sigma}, t) \leq V_2(E, \tilde{W}, \tilde{\mu}, \tilde{\sigma}, 0)$), which implies that $E, \tilde{W}, \tilde{\mu}$ and $\tilde{\sigma}$ are bounded function. Let the function $\Omega \equiv KE^T E \leq -\dot{V}_2(E, \tilde{W}, \tilde{\mu}, \tilde{\sigma}, t)$ and integrate the function $\Omega(t)$ with respect to time yields:

$$\int_0^t \Omega(\tau) d\tau \leq V_2(E, \tilde{W}, \tilde{\mu}, \tilde{\sigma}, 0) - V_2(E, \tilde{W}, \tilde{\mu}, \tilde{\sigma}, t) \quad (65)$$

Since $V_2(E, \tilde{W}, \tilde{\mu}, \tilde{\sigma}, 0)$ is bounded and $V_2(E, \tilde{W}, \tilde{\mu}, \tilde{\sigma}, t)$ is non-increasing and bounded, the following result can be obtained:

$$\lim_{t \rightarrow \infty} \int_0^t \Omega(\tau) d\tau \leq \infty \quad (66)$$

In addition, since all variables in the right hand side of (59) are bounded, it implies \dot{E} is also bounded,

then $\dot{\Omega}(t)$ uniformly continuous [44]. By using Barbalat's Lemma [44], [45], it can be shown that $\lim_{t \rightarrow \infty} \Omega(t) = 0$. That is, $E(t) \rightarrow 0$ as $t \rightarrow \infty$. As a result, the intelligent adaptive control system is asymptotically stable. Moreover, the tracking error of the system will converges to zero according to $E(t) = 0$.

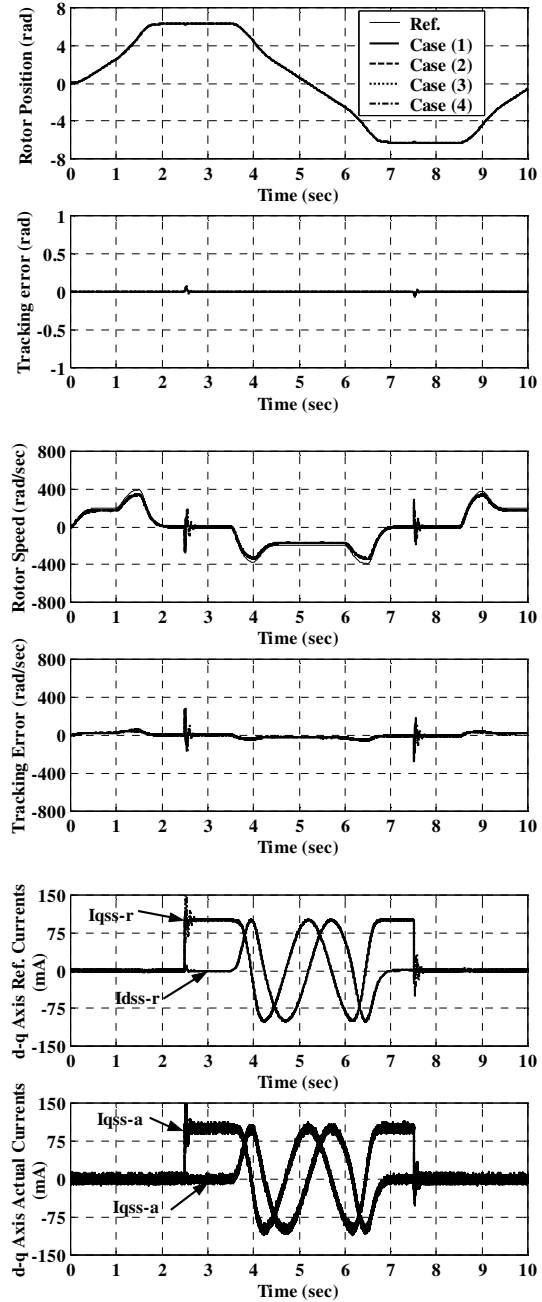


Fig. 10 Dynamic response of the micro-PMSM drive system for a reference model of 2π rad and subsequent loading of 0.5 mNm using IHCS at different cases (1~4) of parameter uncertainties

7 Numerical Simulation Results

In order to investigate the effectiveness of the proposed tracking control scheme, the simulation of the proposed IHCS is carried out using MATLAB/SIMULINK package based on the control system shown in Fig. 1. To demonstrate the control performance of the proposed control scheme for micro-PMSM servo drive system, the simulated results due the tracking of reference model are given. All parameters in the proposed control scheme are chosen to achieve the best dynamic performance.

7.1 Performance Measure of the micro-PMSM Servo Drive System

To measure the performance of the micro-PMSM servo drive system, the maximum tracking error, TE_{max} , the average tracking error, TE_{mean} and the standard deviation of the tracking error, T_{sd} , are defined as follows:

$$TE_{max} = \max_k \sqrt{T(k)^2} \quad (67)$$

$$TE_{mean} = \frac{\sum_{k=1}^n T(k)}{n} \quad (68)$$

$$TE_{sd} = \sqrt{\frac{\sum_{k=1}^n (T(k) - T_{mean})^2}{n}} \quad (69)$$

where $T(k) = [\theta_r^m(k) - \theta_r(k)]$. The comparison of the control performance can be easily demonstrated using (58)-(60).

7.2 Numerical Simulation of the micro-PMSM Servo Drive System

The simulation results of the micro-PMSM servo drive system are presented to verify the feasibility of the proposed IHCS under various operating conditions. To investigate the robustness of the proposed controllers, four cases including parameter uncertainties (PU) and external load disturbance are considered. $\tau_m = (\beta_m / J_m)$ is the mechanical time constant.

Case 1: $1.0 \times (L_s / R_s)$, $1.0 \times (\beta_m / J_m)$, $1.00 \times \lambda_m$, $T_L = 0 - 0.5$ mN.m

Case 2: $0.5 \times (L_s / R_s)$, $1.5 \times (\beta_m / J_m)$, $0.85 \times \lambda_m$, $T_L = 0 - 0.5$ mN.m

Case 3: $1.5 \times (L_s / R_s)$, $2.5 \times (\beta_m / J_m)$, $1.25 \times \lambda_m$, $T_L = 0 - 0.5$ mN.m

Case 4: $1.5 \times (L_s / R_s)$, $5.0 \times (\beta_m / J_m)$, $1.25 \times \lambda_m$, $T_L = 0 - 0.5$ mN.m

The dynamic performance of the micro-PMSM servo drive due to reference model command under subsequent loading of 0.5 mN.m for the CTC at case (1) of PU including the responses of the reference model and rotor position, the tracking position error, rotor speed, the tracking speed error, d-q axis current

response are predicted in Fig. 3, respectively. On the other hand, the dynamic performance using the PRFNNC is shown in Fig. 4 at case (1) of PU. While the dynamic performance using the proposed IHCS is illustrated in Fig. 5 at case (1) of PU. In addition, the disturbance rejection capabilities have been checked when a load of 0.5 mN.m is applied to the shaft at $t=2.5$ sec and removed after a period of 5.0 sec. The results obtained in Figs. 3 and 5 illustrate good dynamic performances, in command tracking and load regulation performance, are realized for the three position tracking controllers. Improvement of the control performance by addition the proposed PRFNNC and IHCS can be observed from the obtained results in command tracking and load regulation characteristics. The comparison between the proposed controllers with the model-following response and load regulation characteristics are given in Figs. 6 and 7. From these results shown in Figs. 6 and 7, the tracking position error and tracking speed error with the CTC is larger than the ones using the PRFNNC and IHCS. In addition, the maximum dip of the rotor position and speed are much reduced utilizing the PRFNNC and IHCS.

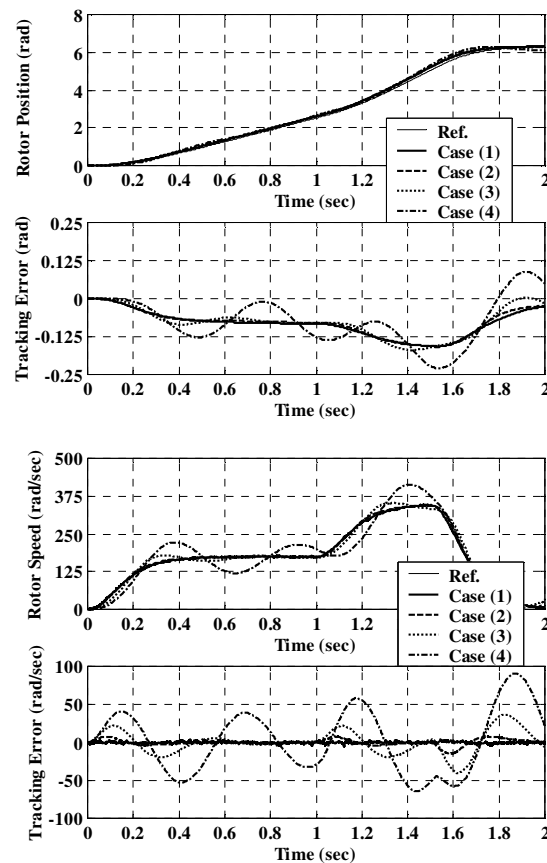


Fig. 11 Enlarge dynamic response for model-following of the micro-PMSM drive system for a reference model of 2π rad using CTC at different cases (1~4) of parameter uncertainties

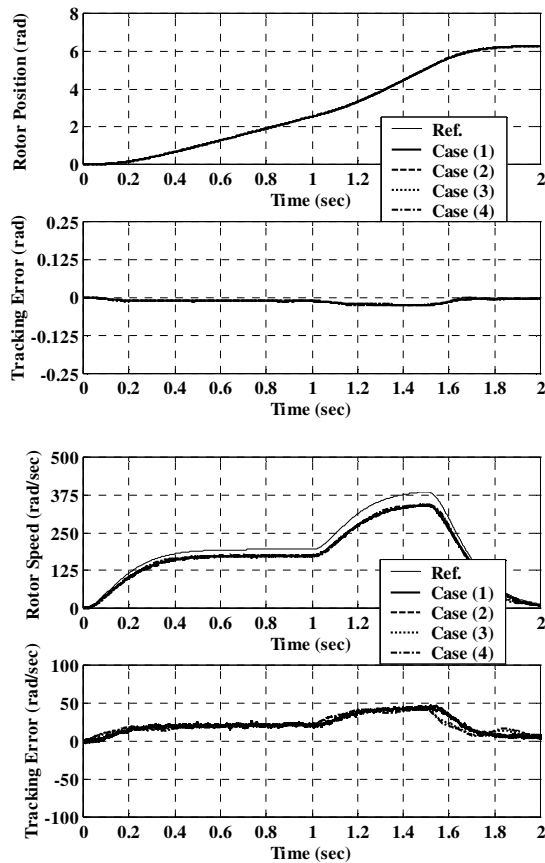


Fig. 12 Enlarge dynamic response for model-following of the micro-PMSM drive system for a reference model of 2π rad using PRFNNC at different cases (1~4) of PU

It is evident that an obvious model-following error (MFE) due to the CTC reaches to -0.16 rad. As well, the CTC returns the position to the reference under full load with a maximum dip of 0.6007 rad and a recovery time of 0.85 sec. On the other hand, favorable tracking response characteristics can be obtained using the proposed PRFNNC and IHCS. The model-following error reaches to -0.005 rad using the PRFNNC. Additionally, the PRFNNC quickly returns the position to the reference under full load with a maximum dip of 0.223 rad and a recovery time of 0.25 sec. While the model-following error reaches to -0.001 rad using the IHCS. Also, the proposed IHCS quickly returns the position to the reference under full load with a maximum dip of 0.0559 rad and a recovery time of 0.06 sec. It is clear from simulation results shown in Figs. 6 and 7 that the CTC provides a slow response for the reference model under full load condition with a long recovery time and a large percentage dipping in the rotor position of about of 9.56% . Whilst the PRFNNC illustrates a fast response reference model under load disturbance with a short recovery time and a maximum dipping in the rotor position of

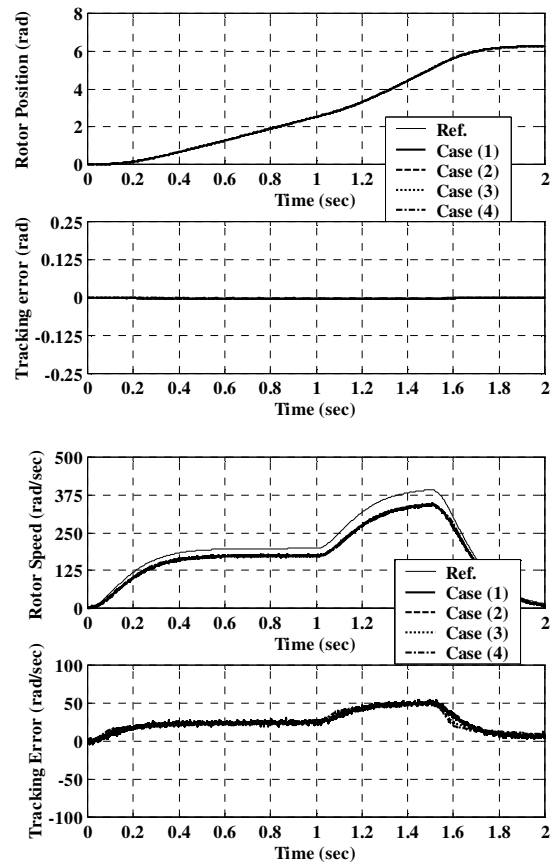


Fig. 13 Enlarge dynamic response for model-following of the micro-PMSM drive system for a reference model of 2π rad using IHCS at different cases (1~4) of PU

about 3.45% . At the same time, the proposed IHCS shows the robust performance in model-following tracking and load regulation characteristics with a very fast recovery time and a maximum dipping in the rotor position of about 0.89% .

To further verify the performance robustness of the proposed control schemes, four cases of PU and external load disturbance are considered, case (1~4), for comparison. The dynamic performances of the micro-PMSM servo drive for position controllers at all cases of PU are predicted in Figs. 8, 9 and 10. Enlarge of the dynamic response for model following and load regulation characteristics are illustrated in Figs. 11, 12, 13, 14, 15 and 16. From the simulation results shown in Figs. (11-16), the tracking errors converge quickly and the robust control characteristics of the proposed IHCS under the occurrence of PU can be clearly observed. Compared with the CTC and PRFNNC, the tracking errors and regulation characteristics are much reduced. Therefore, the proposed IHCS can yield superior control performance than the CTC and PRFNNC control schemes. As a result, the proposed IHCS provides a rapid and accurate response for the

reference model under load changes within 0.2 sec compared with the CTC and PRFNNC. The CTC has sluggish recovery time of more than 3.0 sec at PU and the PRFNNC has a recovery time of about 1.5 sec. Thus, it can be verified that the proposed IHCS at all cases of PU can satisfy the robustness, the accuracy requirements and is more suitable in the tracking control of the micro-PMSM servo drive for different applications.

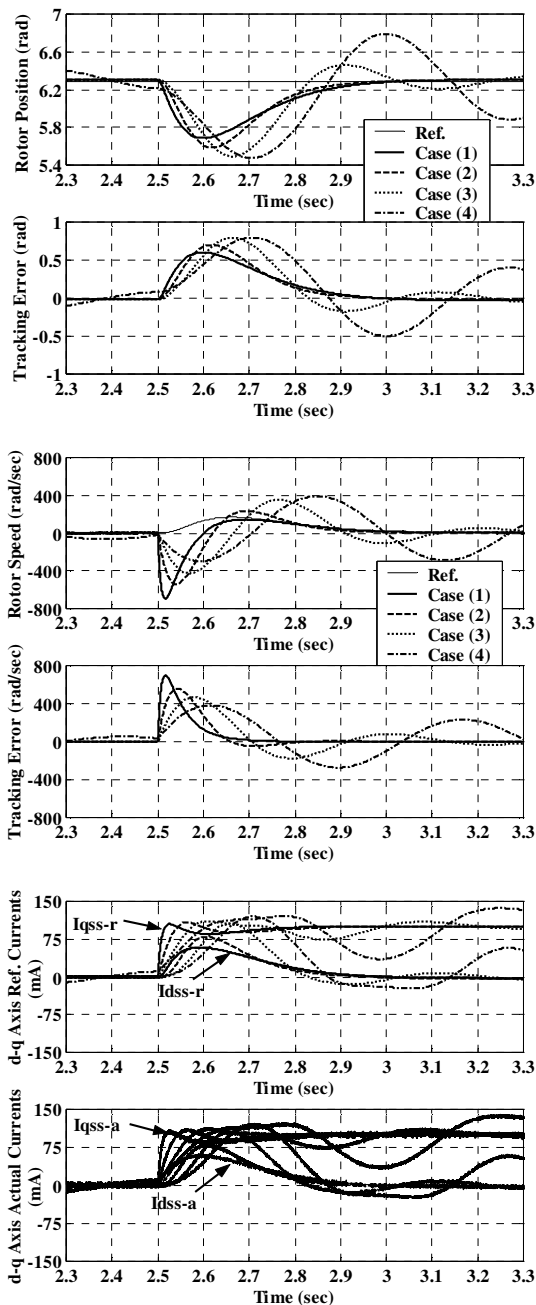


Fig. 14 Enlarge dynamic response for load regulation of the micro-PMSM drive system for a reference model of 2π rad and subsequent loading of 0.5 mNm using CTC at different cases (1~4) of parameter uncertainties

The performance measures of the CTC, PRFNNC and IHCS using maximum tracking error, average tracking error and standard deviation of the tracking error given in (67)-(69), are shown in Tables 2, 3 and 4 at nominal parameters, case (1), and at parameter variations (cases (2~4)) for the comparison of the control performance of the micro-PMSM servo drive. Comparing the performance measures shown in Tables 2, 3 and 4, at case (1), the averages of the maximum, average and standard deviation tracking errors of the proposed PRFNNC are reduced by 62.91%, 91.19% and 79.40%, respectively with respect to CTC. The percentage reduction in the tracking errors using the proposed IHCS are 90.70%, 98.54% and 96.70%%, respectively with respect to CTC. Additionally, at parameter variations cases, Tables 5 and 6 illustrate these percentage reductions in the maximum tracking error, average tracking error and standard deviation of the tracking error using the PRFNNC and IHCS with respect to the CTC scheme. Finally, it is obvious that all the performance measures are improved greatly by using the IHCS. Therefore, the proposed IHCS possesses better performance apparently and is robust with regard to load disturbance and PU.

7.3 Control Performance Comparison for the micro-PMSM Servo Drive System

To further investigate the improvement of the control performance using the proposed IHCS, the performance measures of the CTC, PRFNNC and IHCS at the four cases of PU are compared using the percentage of the tracking error reductions with respect to CTC. The percentage reductions in the tracking errors for both PRFNNC and IHCS with respect to CTC control scheme are given in Figs. 17 and 18. From the results, one can easily observe that all values of TE_{max} , TE_{mean} and TE_{sd} have been successfully reduced by the proposed IHCS.

Table 2 Performance measures of the CTC under PU of the micro-PMSM servo drive system

Parameters Uncertainties	Tracking Errors (rad)		
	Maximum	Average	S.D.
Case (1)	0.6013	0.0014230	0.1302
Case (2)	0.7010	0.0010520	0.1365
Case (3)	0.7938	0.0009263	0.1549
Case (4)	0.7961	0.0005446	0.2210

Table 3 Performance measures of the PRFNNC under PU of the micro-PMSM servo drive system

Parameters Uncertainties	Tracking Errors (rad)		
	Maximum	Average	S.D.
Case (1)	0.2230	0.00012530	0.02682
Case (2)	0.2324	0.00013540	0.02765
Case (3)	0.2711	0.00013840	0.03624
Case (4)	0.2767	0.00013550	0.04122

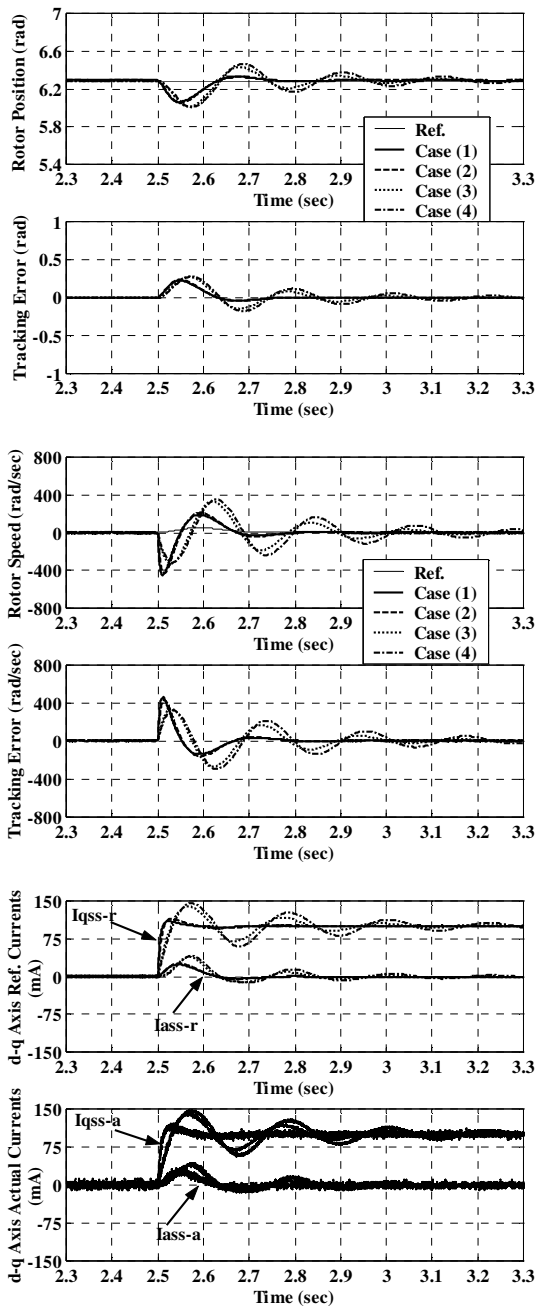


Fig. 15 Enlarge dynamic response for load regulation of the micro-PMSM drive system for a reference model of 2π rad and subsequent loading of 0.5 mNm using PRFNNC at different Cases (1~4) of parameter uncertainties

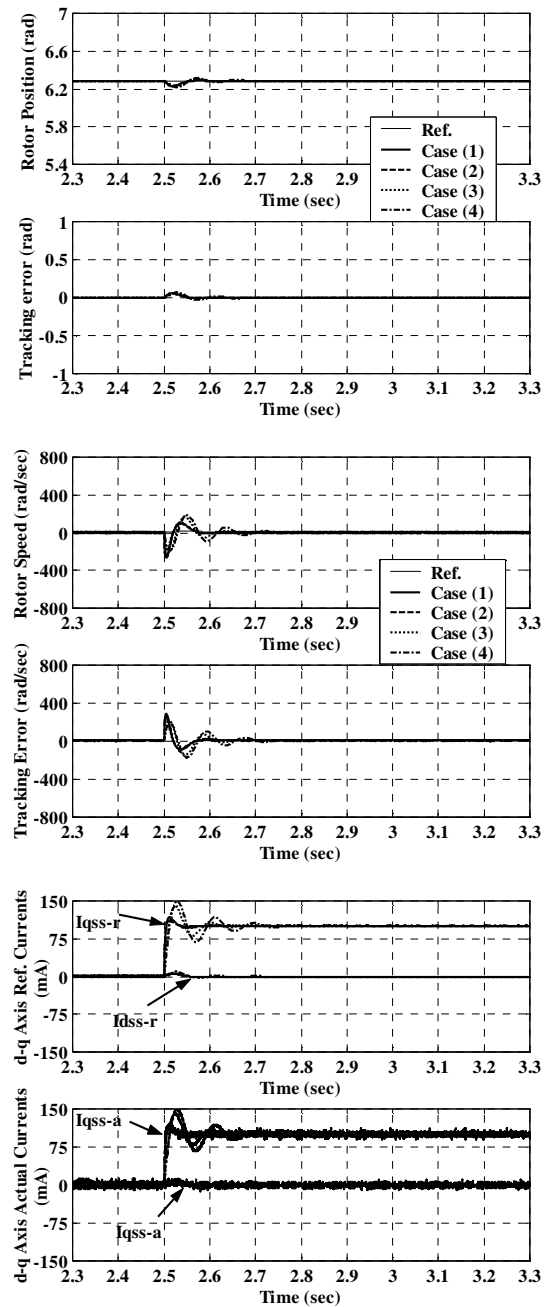


Fig. 16 Enlarge dynamic response for load regulation of the micro-PMSM drive system for a reference model of 2π rad and subsequent loading of 0.5 mNm using IHCS at different Cases (1~4) of parameter uncertainties

Table 4 Performance measures of the IHCS under PU for the micro-PMSM servo drive system

Parameters Uncertainties	Tracking Errors (rad)		
	Maximum	Average	S.D.
Case (1)	0.05590	2.072e-005	0.004301
Case (2)	0.05409	1.652e-005	0.004241
Case (3)	0.06484	2.195e-005	0.005011
Case (4)	0.06710	2.065e-005	0.005577

Table 5 Tracking position errors reduction using PRFNNC with respect to CTC under PU for the micro-PMSM servo drive system

Parameters Uncertainties	Tracking Errors Reduction (%)		
	Maximum	Average	S.D.
Case (1)	62.91	91.19	79.40
Case (2)	66.85	87.13	79.74
Case (3)	65.85	85.06	76.60
Case (4)	65.24	75.12	81.35

Table 6 Tracking position errors reduction using IHCS with respect to CTC under PU of micro-PMSM servo drive system

Parameters Uncertainties	Tracking Errors Reduction (%)		
	Maximum	Average	S.D.
Case (1)	90.70	98.54	96.70
Case (2)	92.28	98.43	96.89
Case (3)	91.83	97.63	96.77
Case (4)	91.57	96.21	97.48

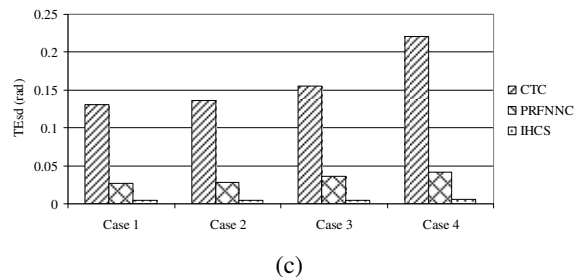
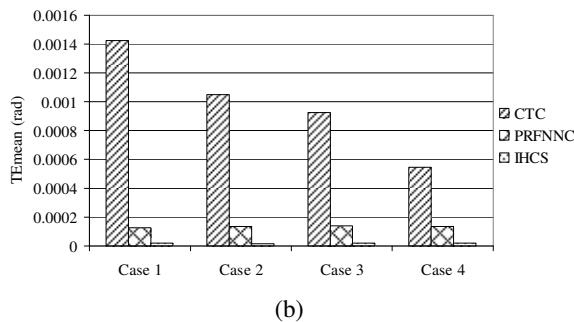
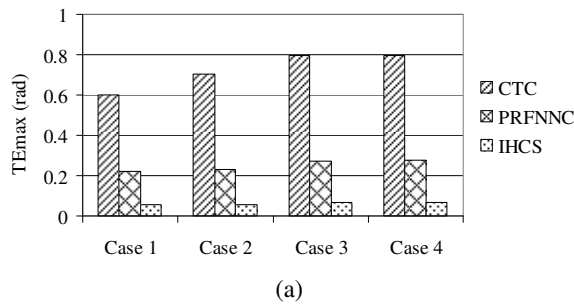


Fig. 17 Performance measures of CTC, PRFNNC and IHCS for micro-PMSM servo drive
(a) TE_{max} (b) TE_{mean} (c) TE_{sd}

8 Conclusions

This paper proposed an IHCS for micro-PMSM servo drive which guarantees the robustness in the presence of parameter uncertainties and load disturbances. The proposed control scheme comprises a CTC based on the sliding-mode technique, a PRFNNC and a PRFNNI. First, the CTC is designed to stabilize the micro-PMSM servo drive system. Then, to improve the robustness of the micro-PMSM servo drive system due to the parameter uncertainties an IHCS is proposed. The IHCS combines the PRFNNC and PRFNNI. The

PRFNNC is used as the main tracking controller to mimic the CTC law and to preserve favorable model-following characteristics while the PRFNNI is utilized to identify the sensitivity information of the micro-PMSM servo drive system required for the PRFNNC. The online adaptive control laws are derived based on the Lyapunov stability theorem, the Taylor linearization technique and the back propagation method so that the stability of the micro-PMSM servo drive system can be guaranteed under occurrence of servo drive uncertainties. The simulated results due to reference model trajectory confirm that the proposed IHCS grants robust performance and precise dynamic response to the reference model regardless of load disturbances and micro-PMSM parameter uncertainties. Finally, the main contribution of this paper is the successful development and application of the IHCS with adaptive PRFNNC methodology to control the rotor position of the load disturbances and parameters uncertainties.

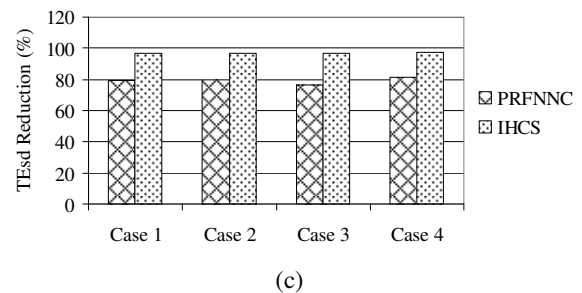
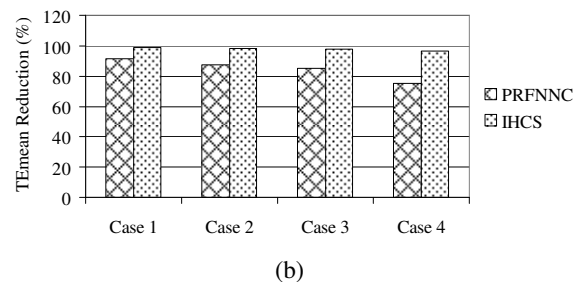
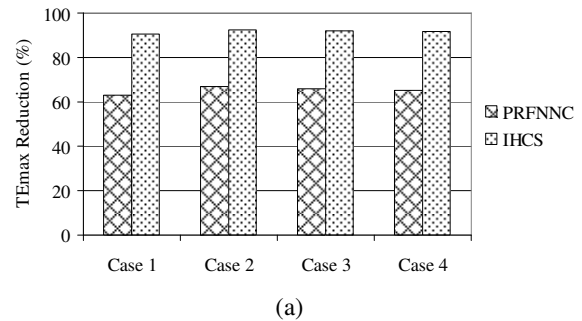


Fig. 18 Tracking errors reduction using CTC, PRFNNC and IHCS for micro-PMSM servo drive
(a) TE_{max} red. (b) TE_{mean} red. (c) TE_{sd} red.

References:

- [1] K. Hameyer, and R. Belmans, Design of very small electromagnetic and electrostatic micro motors, *IEEE Trans. Energy Convers.*, Vol. 14, No. 4, 1999, pp. 1241–1246.
- [2] P.L. Chapman and P.T. Krein, Smaller is better? [micromotors and electric drives], *IEEE Ind. Appl. Mag.*, Vol. 9, No. 1, 2003, pp. 62–67.
- [3] D. P. Arnold, N. Wang, Permanent magnets for MEMS, *J. Mechtron. Sys.*, Vol. 18, No. 6, pp. 1255-1266, 2009.
- [4] H. Ishihara, F. Arai, T. Fukuda, Micro Mechatronics and Micro Actuators, *IEEE/ASME Trans. Mechtron.*, Vol. 1, No. 1, 1996, pp. 68-79.
- [5] Hur Koser and Jeffrey H. Lang, Magnetic Induction Micromachine—Part I: Design and Analysis, *IEEE J. Microelectromech. Syst.*, Vol. 15, No. 2, 2006, pp. 415-426.
- [6] Florent Cros, Hur Koser, Mark G. Allen and Jeffrey H. Lang, Magnetic Induction Micromachine—Part II: Fabrication and Testing, *IEEE J. Microelectromech. Syst.*, Vol. 15, No. 2, 2006, pp. 427-439.
- [7] H. Koser, J.H. Lang, Magnetic induction micro machine—part III: eddy currents and nonlinear effects, *IEEE J. Microelectromech. Syst.*, Vol. 15, No. 2, 2006, pp. 440–456.
- [8] Steven F. Nagle, Carol Livermore, Luc G. Frechette, Reza Ghodssi, and Jeffrey H. Lang, An Electric Induction Micromotor, *IEEE J. Microelectromech. Syst.*, Vol. 14, No. 5, 2005, pp. 1127-1143.
- [9] M. Feldmann, S. Buttgenbach, Linear variable reluctance (VR) micro motors with compensated attraction force: concept, simulation, fabrication and test, *IEEE Trans. Mag.*, Vol. 43, No. 6, 2007, pp. 2567–2569.
- [10] I.S. Jung, J.H. Kim, J.H. Choi, H.G. Sung, A six-phase multilevel inverter for MEMS electrostatic induction micromotors, *IEEE Trans. Circuits Syst.*, Vol. 51, No. 2, 2004, pp. 49–56.
- [11] J. Zhang, M. Schroff, High-performance micromotor control systems, *IEEE IECON*, 2003, pp. 347–352.
- [12] J. Zhang, Q. Jiang, Sensorless commutation of micro PMSMs for high-performance high-speed applications, *IEEE ICEMS*, 2005, pp. 1795–1800.
- [13] Y.H. Chang, T.H. Liu, C.C. Wu, Design and implementation of an H_∞ controller for a micropermanent-magnet synchronous motor position control system, *IET Electr. Power Appl.*, Vol. 2, No. 1, 2008, pp. 8–18.
- [14] Y.H. Chang, T.H. Liu, C.C. Wu, Novel adjustable micropermanent-magnet synchronous motor control system without using a rotor-position/speed sensor, *IEE Proc. Electr. Power Appl.*, Vol. 153, No. 3, 2006, pp. 429–438.
- [15] Y.H. Chang, T.H. Liu, D. F. Chen, Design and implementation of a robust controller for a micro permanent magnet synchronous speed control systems, *IEEE ICICIC*, 2007.
- [16] D. Polla, A. Erdman, D. Peichel, R. Rizq, Y. Gao, and D. Markus, Precision micromotor for surgery, *IEEE MMB*, 2000, pp. 180–183.
- [17] J. Hur, S.H. Rhyu, I.S. Jung, H.G. Sung and B.I. Kwon, Three-dimensional characteristic analysis of micro BLDC motor according to slotless winding shape, *IEEE Trans. Magn.*, Vol. 39, No. 5, , 2003 pp. 2989–2991.
- [18] H. Lu, J. Zhu and Y. Guo, A permanent magnet linear motor for micro robots, *IEEE PEDS*, 2005, pp. 590–595.
- [19] S.E. Lysheski, Mini- and micro scale closed-loop servo drivers with brushless mini motors and ICs monolithic amplifiers/controllers, *IEEE CDC*, 2002, pp. 3670–3674.
- [20] A. Purushotham, S.L. Garverick, C. Edwards and M.L. Nagy, A closed-loop micro motor control system', *IEEE ISCAS*, 1996, pp. 209–212.
- [21] F. F. M. El-Sousy, Robust Petri Recurrent-Fuzzy-Neural-Network Sliding-Mode Control for Micro-PMSM Servo Drive System, 8th WSEAS International Conference on Dynamical Systems and Control, Porto, Portugal, July 1-3, 2012, pp. 66-75.
- [22] Y.H. Chang, T.H. Liu, D. F. Chen, Design and implementation of an adaptive inverse controller for a micro-permanent magnet synchronous control system, *IET. Electr. Power Appl.*, 2009, Vol. 3, No. 5, pp. 471–481.
- [23] T.Y. Chou , T.H. Liu, T.T. Cheng, Sensorless micro-permanent magnet synchronous motor control system with a wide adjustable speed range, *IET. Electr. Power Appl.*, Vol. 6, No. 2, 2012, pp. 62–72.
- [24] T.Y. Chou , T.H. Liu, Implementation of a motion control system using micro-permanent magnet synchronous motors, *IET. Electr. Power Appl.*, Vol. 6, No. 6, 2012, pp. 362–374.
- [25] Y. G. Leu, T. T. Lee and W. Y. Wang, On-line tuning of fuzzy-neural network for adaptive control of nonlinear dynamical systems, *IEEE Trans. Syst., Man, Cybern.*, Vol. 27, No. 6, 1997, pp. 1034-1043.
- [26] Y. S. Lu and J. S. Chen, A self-organizing fuzzy sliding-mode controller design for a class of nonlinear servo systems, *IEEE Trans.*

- Indust. Electron.*, Vol. 41, No. 5, 1994, pp. 492–502.
- [27] C. H. Lee and C.C. Teng, Identification and Control of Dynamic Systems Using Recurrent-Fuzzy-Neural-Network, *IEEE Trans. on Fuzzy Syst.*, Vol. 8, No. 4, 2000, pp. 349-366.
- [28] W. Y. Wang, Y. G. Leu, and C. C. Hsu, Robust adaptive fuzzy-neural control of nonlinear dynamical systems using generalized projection update law and variable structure controller, *IEEE Trans. Syst., Man, Cybern. B*, Vol. 31, No. 1, 2001, pp. 140–147.
- [29] C. H. Wang, H. L. Liu, and T. C. Lin, Direct adaptive fuzzy-neural control with state observer and supervisory controller for unknown nonlinear dynamical systems, *IEEE Trans. Fuzzy Syst.*, Vol. 10, No. 1, 2002, pp. 39–49.
- [30] Y. G. Leu, W. Y. Wang, and T. T. Lee, Robust adaptive fuzzy-neural controllers for uncertain nonlinear systems, *IEEE Trans. Robot. Automat.*, Vol. 15, No. 5, 1999, pp. 805–817.
- [31] J. Zhang and A. J. Morris, Recurrent neuro-fuzzy networks for nonlinear process modeling, *IEEE Trans. Neural Networks*, Vol. 10, No. 2, 1999, pp. 313–326.
- [32] C. F. Hsu and K. H. Cheng, Recurrent Fuzzy-Neural approach for nonlinear control using dynamic structure learning scheme, *Neurocomputing*, Vol. 71, No. (16-18), 2008, pp. 3447-3459.
- [33] W. Pedrycz and F. Gomide, A Generalized Fuzzy Petri Nets, *IEEE Transaction on Fuzzy Systems*, Vol. 2, No. 4, 1994, pp. 295-301.
- [34] M. Gao, M. C. Zhou, X. Haugand Z. Wu, Fuzzy reasoning Petri Nets, *IEEE Trans. Syst., Man, Cybern. A*, Vol. 33, No. 3, 2003, pp. 314–324.
- [35] R. David and H. Alla, Petri nets for modeling of dynamic systems-A survey” *Automatica*, Vol. 30, No. 2, 1994, pp. 175–202.
- [36] T. Murata, Petri nets: Properties, analysis and applications, *Proc. IEEE*, Vol. 77, No. 4, 1989, pp. 541–580.
- [37] L. Xiaoou, Y. Wen, and F. Lara-Rosano, Dynamic knowledge inference and learning under adaptive fuzzy Petri net framework, *IEEE Trans. Syst., Man, Cybern. C*, Vol. 30, No. 4, 2000, pp. 442–450.
- [38] V. R. L. Shen., Reinforcement learning for high-level fuzzy Petri nets, *IEEE Trans. Syst., Man, Cybern. B*, Vol. 33, No. 2, 2003, pp. 351–362.
- [39] K. Hirasawa, M. Ohbayashi, S. Sakai, and J. Hu, Learning Petri network and its application to nonlinear system control, *IEEE Trans. Syst., Man, Cybern. B*, Vol. 28, No. 6, 1998, pp. 781–789.
- [40] S. I. Ahson, Petri net models of fuzzy neural networks, *IEEE Trans. Syst., Man, Cybern.*, Vol. 25, No. 6, 1995, pp. 926–932.
- [41] M. Hanna, A. Buck, and R. Smith, Fuzzy Petri nets with neural networks to model products quality from a CNC-milling machining centre, *IEEE Trans. Syst., Man, Cybern. A*, Vol. 26, No. 5, 1996, pp. 638–645.
- [42] R. J. Wai and C. M. Liu, Design of Dynamic Petri Recurrent Fuzzy Neural Network and Its Application to Path-Tracking Control of Nonholonomic Mobile Robot, *IEEE Trans. Ind. Electron.*, Vol. 56, No. 7, 2009, pp. 2667–2683.
- [43] C. T. Lin and C. S. G. Lee, *Neural Fuzzy System: A Neural-Fuzzy Synergism to Intelligent System*, Englewood cliffs, NJ: Prentice-Hall, 1996.
- [44] J. J. E. Slotine and W. LI, *Applied Nonlinear Control*, Prentice-Hall, New Jersey, 1991.
- [45] K. J. Astrom and B. Wittenmark, *Adaptive Control*, Addison-Wesley, New York, 1995.
- [47] Wen-Chun Chi, Ming-Yang Cheng, Implementation of a sliding-mode-based position sensorless drive for high-speed micro permanent-magnet synchronous motors, *ISA Trans.*, Vol. 53, No. 2, 2014, pp. 444–453.